Reduced intestinal GLP-1$^+$ cell numbers are associated with an inflammation-related epithelial metabolic signature

Short title: Reduced GLP-1$^+$ cells in gut inflammation

Elisabeth Urbauer[1], Doriane Aguanno[1], Katharina Kuellmer[2], Amira Metwaly[1], Nadine Waldschmitt[1], Mohamed Ahmed[1], Sevana Khaloian[1], Gabriele Hörmannsperger[1], Julien Planchais[3], Tobias Fromme[2,4], R Balfour Sartor[5], Harry Sokol[3,6,7], Dirk Haller[1,8], Eva Rath[1*]

[1]Chair of Nutrition and Immunology, School of Life Sciences, Technical University of Munich, Freising, Germany

[2]Chair of Molecular Nutritional Medicine, School of Life Sciences, Technical University of Munich, Freising, Germany

[3]Micalis Institute, INRA, AgroParisTech, Université Paris-Saclay, Jouy-en-Josas, France

[4]EKFZ-Else Kröner-Fresenius Center for Nutritional Medicine, Technical University of Munich, Freising, Germany

[5]Department of Medicine, Center for Gastrointestinal Biology and Disease, University of North Carolina at Chapel Hill, Chapel Hill, North Carolina, USA.

[6]Sorbonne Université, INSERM, Centre de Recherche Saint-Antoine, CRSA, AP-HP, Saint-Antoine Hospital, Gastroenterology Department, 75012 Paris, France

[7]Paris Center for Microbiome Medicine (PaCeMM) FHU, Paris, France

[8]ZIEL Institute for Food and Health, Technische Universität München, Freising, Germany

* Correspondence: Eva Rath, TUM SoLS, Gregor-Mendel Str. 2, 85354 Freising eva.rath@tum.de

Disclosures: *The authors declare that the research was conducted in the absence of any commercial or financial relationships that could be construed as a potential conflict of interest*.

Grant support: NIH P40OD01995, P30DK034987, P01DK94779 (RBS), Crohn's & Colitis Foundation (RBS)

Data Transparency: All data generated or analyzed during this study are included in this published article. Additional datasets, including raw data, are available from the corresponding author upon reasonable request.

Synopsis: This study examines GLP-1^{+} cells in intestinal inflammation, showing consistent reductions in inflamed areas. Findings from mouse models and human data reveal an inflammatory metabolic profile linked to altered epithelial differentiation. GLP-1, involved in endocrine-immune crosstalk, may impact mucosal inflammation and symptoms, making it a therapeutic target.

Graphical Abstract:

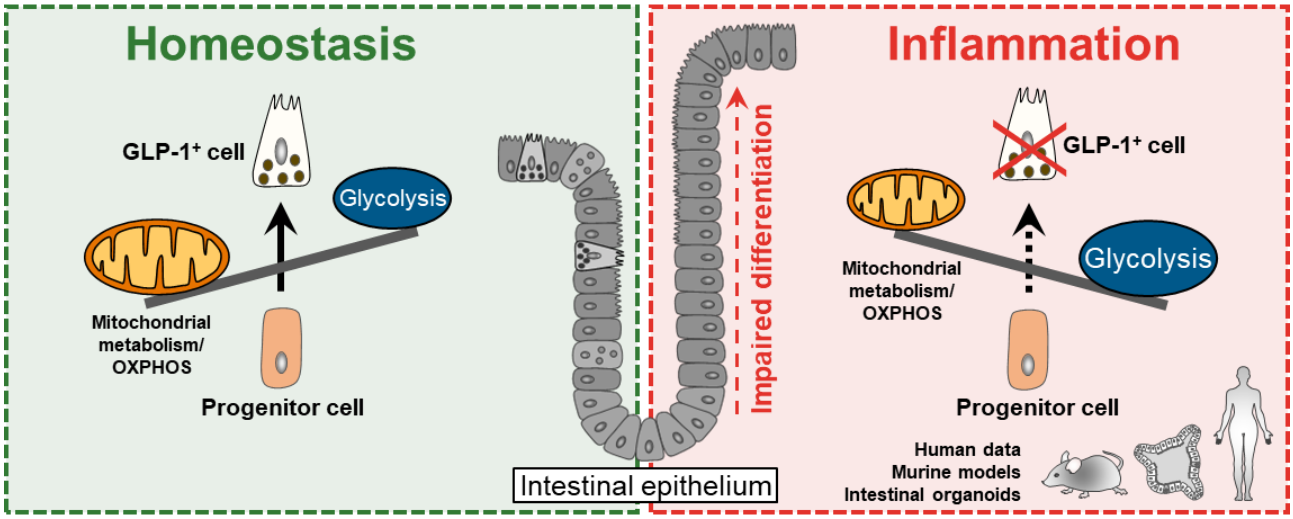

Abbreviations:

AMPK	5'-prime-AMP-activated protein kinase
Atf/ ATF	Activating transcription factor
ATP	Adenosine triphosphate
CCK	Cholecystokinin
CD	Crohn´s disease
ClpP	Caseinolytic mitochondrial matrix peptidase
Dclk	Doublecortin-like kinase protein
EEC	Enteroendocrine cell
Gcg/ GCG	Glucagon
GLP	Glucose like protein
Hmgcs2/ HMGCS2	3-Hydroxy-3-methylglutaryl-CoA synthase
HS	Histoscore
IBD	Inflammatory bowel diseases
IEC	Intestinal epithelial cell
IL	Interleukin
Isl	Insulin gene enhancer protein
Mtor	Mechanistic target of Rapamycin
Ngn	Neurogenin
Pax	Paired box
PRKAA	Protein kinase AMP-activated catalytic subunit alpha
Tnf	Tumor necrosis factor
TPH	Tryptophan hydroxylase
Trib/TRIB	Tribbles pseudokinase
UC	Ulcerative colitis
Wt	Wild type

Abstract

Background & Aims While hormone secretion from enteroendocrine cells (EECs) and their functions in digestion and metabolism are well studied, the role of EECs in intestinal inflammation is virtually unknown. In inflammatory bowel diseases (IBD), a contribution of EECs to pathogenesis is indicated by autoantibodies affecting EEC function and general disease symptoms like insulin resistance and altered intestinal motility. Particularly, the L cell-derived hormone glucagon-like peptide 1 (GLP-1) exerts direct effects on intraepithelial lymphocytes and is suggested to orchestrate metabolic-inflammatory responses. However, the role of EECs in intestinal inflammation is poorly understood.

Methods We quantified numbers of GLP-1^{+} cells in 4 different mouse models of intestinal inflammation and performed transcriptional analyses of colonic epithelial cells from inflamed interleukin (IL)10-deficient mice. Using a publicly available single-cell RNA sequencing dataset including mucosal biopsies from Crohn´s disease (CD) patients, we confirmed findings from the murine models. A model of mitochondrial dysfunction (ClpP$^{\Delta IEC}$ mice) as well as murine and human intestinal organoids were used to study molecular mechanisms.

Results Numbers of GLP-1 expressing cells are consistently reduced at the site of active disease in mouse models of intestinal inflammation and CD patients. Colonic L cells from inflamed IL-10$^{-/-}$ mice remained functional in terms of hormone secretion. Transcriptional analyses of intestinal epithelial cells indicate altered epithelial differentiation correlating with an inflammatory metabolic fingerprint. Reduced GLP-1^{+} cells in ClpP$^{\Delta IEC}$ mice and inhibition of respiration in organoid cultures supports a causative role for metabolism in steering differentiation.

Conclusion Reduction of GLP-1^{+} cells represents a general feature of ileal and colonic inflammation in mice and human. Given the numerous properties of GLP-1, this reduction likely affects inflammatory processes in the mucosa and disease-related symptoms on multiple levels, and therefore, should be considered a therapeutic target in IBD.

Keywords: Glucagon-like peptide 1; L cells; Enteroendocrine cells; inflammatory bowel diseases

1 Introduction

Enteroendocrine cells (EECs) are renowned for regulating gastrointestinal motility, secretion of digestive fluids, and inducing insulin release *via* peptide hormones. In particular, glucagon-like peptide 1 (GLP-1) has gained enormous attention due to its insulinotropic action and relevance in the treatment of type 2 diabetes and obesity (1). EECs constitute approximately 1% of intestinal epithelial cells (IECs) and are scattered throughout the intestine (2). The intestinal epithelium itself is a key player in maintaining metabolic and immune homeostasis. Ensuring efficient nutrient absorption and at the same time forming a barrier for host defense (3), IECs constitute the body´s most important and dynamic interface to the external environment (4). Stem cells localized at the crypt base expressing leucine-rich repeat-containing G-protein coupled receptor 5 (Lgr5) constantly divide and renew the IEC layer within 3-5 days (5), giving rise to different subtypes of IECs. These subtypes, comprising enterocytes, Paneth cells, goblet cells, tuft cells, M cells, and EECs (6), fulfill specialized functions, with absorptive enterocytes and secretory (mucin-producing) goblet and (antimicrobial peptides-producing) Paneth cells accounting for the largest proportion of IECs.

The regulation of stem cell renewal, proliferation and differentiation is of particular importance under pathological conditions, such as wound healing, tissue regeneration and acute and chronic inflammation as seen in inflammatory bowel diseases (IBD). IBD comprises ulcerative colitis (UC) and Crohn’s disease (CD), which are characterized by relapsing inflammation of the colon (UC) or different areas of the gastrointestinal tract but predominantly affecting the terminal ileum (CD). The current paradigm for IBD pathogenesis is a dysregulated interaction between the intestinal microbiota and the mucosal immune system. Consequently, failure of IECs as mediators between these two major factors influencing intestinal inflammation (3) may critically contribute to IBD pathogenesis (7).

Alterations in IEC subpopulations and aberrances of the intestinal stem cell niche have been described in the context of intestinal inflammation. The reduction of secretory goblet cells and Paneth cells (7-9) are the best-studied phenomena in this context. However, upon parasite infection increases in tuft cells,

CCK-positive cells, and serotonin (5-HT)-producing enterochromaffin cells are also observed (10-12). Yet, GLP-1-expressing L cells as additional members of the secretory linage of IECs have not been thoroughly characterized under inflammatory conditions.

Loss of goblet cells and Paneth cells are early events in intestinal inflammation (9, 13) and have been associated with impaired metabolic fitness of IECs (9, 14). In general, the cellular metabolism plays a pivotal role in regulating intestinal epithelial cell proliferation and differentiation, and mitochondrial function actively determines cellular phenotypes and lineage commitment (9, 15-17). Consistently, there is extensive evidence for altered cellular metabolism, mitochondrial dysfunction, and activation of mitochondrial stress signaling in IBD (15, 18, 19). Moreover, genetic risk loci associated with IBD have been mapped to mitochondrial function-associated genes (15, 20-23) and mitochondrial dysfunction-associated aberrances of the intestinal stem cell niche predict disease recurrence in CD patients (9), suggesting alterations in epithelial cell oxidative metabolism not only as a consequence but causal factor in the development of chronic intestinal inflammation.

Even though EECs have been identified as source of the disease-relevant cytokine IL-17C in IBD (24), and autoantibodies against the enteroendocrine protein UbE4A are associated with disease behavior (25), studies investigating the role of EECs in IBD pathogenesis are scarce. Yet, particularly GLP-1 producing cells might be of interest in the context of inflammation as these cells actively sense the microbiota and bacterial products, and in addition to its role in glucose metabolism, GLP-1 exerts potent anti-inflammatory effects (26, 27). Highlighting the crosstalk between the immune and endocrine system, the GLP-1 receptor is expressed on multiple immune cell populations, including intestinal intraepithelial lymphocytes (28, 29). In addition, general disease symptoms including reduced appetite, anorexia and altered intestinal motility often accompanying intestinal inflammation, might be linked to GLP-1 signaling (2, 30, 31).

As the total number of studies investigating GLP-1^{+} cell numbers and function in the context of intestinal inflammation is limited and results are conflicting (26, 27, 32-34), we quantified numbers of

GLP-1 expressing cells in 4 different mouse models of ileal and colonic inflammation (*Tnf*$^{\Delta ARE}$ mice (ileitis), IL-10$^{-/-}$ mice and adoptive T cell-transfer model (colitis) as well as *Citrobacter rodentium*-infection (colitis)). Consistent across all models, a reduction of GLP-1^{+} cells confined to the site of active inflammation is evident, which occurs early in the course of inflammation. The remaining GLP-1-expressing L cells in IL-10$^{-/-}$ mice are functional in terms of hormone secretion. Importantly, analysis of a recently published data set from single-cell RNA sequencing of mucosal biopsies from CD patients (35), confirmed the human relevance of these findings. In parallel to EEC loss, colonic IECs of inflamed IL-10$^{-/-}$ mice display a metabolic fingerprint that has been associated with reduced differentiation into other cell types of the secretory lineage (goblet cells, Paneth cells). Remarkably, compromised mitochondrial function in ClpP$^{\Delta IEC}$ mice, as well as inhibition of mitochondrial respiration using oligomycin in murine and human organoid cultures was sufficient to reduce EEC marker gene expression, indicating a causative role for metabolism in steering differentiation into this IEC subtype.

2 Results and discussion

2.1 GLP-1 positive cells are consistently reduced under inflammatory conditions

To comprehensively characterize the impact of intestinal inflammation on the number of GLP-1-expressing L cells in the epithelium, ileal and colonic tissue sections from different mouse models of intestinal inflammation were immunohistochemically stained (**Figure 1A**). Cells positive for GLP-1 were quantified as positive cells over the total epithelial layer (mm^2), to minimize confounders due to architectural changes of the intestinal tissue caused by inflammatory processes such as immune cell infiltration. At least 3 non-consecutive, well-oriented tissue sections per mouse were used for quantification. Group sizes were ≥ 5 in all cases. In accordance with 3R principles, tissue samples analyzed were obtained from our tissue biobank and originated from previous studies (9, 36-38). Mouse models investigated comprise commonly used models of IBD, (I) the *Tnf*$^{\Delta ARE}$ mouse model of ileitis and (II) IL-10 deficient mice as model of colitis; (III) an adoptive T cell transfer model of colitis, Rag2$^{-/-}$ mice reconstituted with CD4^{+} CD25^{-} T cells; and (IV) an infection model using *Citrobacter rodentium*. In *Tnf*$^{\Delta ARE}$ mice, CD-like tissue inflammation develops gradually and microbiota-dependent due to loss of translational control of the pro-inflammatory cytokine tumor necrosis factor (Tnf) caused by a deletion of AU-rich (adenosin-uracil) elements (ARE) in the *Tnf* gene/ mRNA, resulting in Tnf overexpression (39). Similarly, mice lacking the anti-inflammatory cytokine interleukin 10 (IL-10$^{-/-}$ mice) spontaneously develop colitis after weaning whereby onset and severity of inflammation are dependent on the microbiota and the genetic background of mice (40), with the 129/SvEv mouse line being more susceptible than C57BL/6 mice. In the following, "IL-10$^{-/-}$ mice" refers to inflamed 129/SvEv IL-10 deficient mice unless otherwise stated. The T cell transfer model of colitis is the most widely used model of IBD to dissect the contribution of T cells to immunopathology in chronic colitis (41). Notably, the expansion of enterochromaffin cells, a cell type closely related to EECs, is dependent on T cell presence during helminth infection (10), indicating a direct effect of immune cells on epithelial cell composition. In contrast to the models of chronic inflammation, infection with *C.*

rodentium causes transient colonic inflammation and hyperplasia and serves as a model to study host-pathogen interaction in the context of IBD and to study molecular mechanisms of human gastrointestinal infections with pathogenic *Escherichia coli* strains (42).

In a first approach, we compared moderately inflamed mice (histopathological score (HS) 2-4) of the different models to wild type (Wt) littermates or non-reconstituted/ non-infected mice, respectively (**Figure 1B-E**). Consistently throughout all models investigated, numbers of GLP-1^{+} cells were reduced under inflammatory conditions (**Figure 1B-E**). These changes were observed at the site of active disease, namely the ileum in *Tnf*$^{\Delta ARE}$ mice (**Figure 1B**) and the colon in IL-10$^{-/-}$ mice, Rag2$^{-/-}$ mice adoptively transferred with colitogenic CD4^{+} CD25^{-} T cells, and C57BL/6 mice infected with *C. rodentium* (**Figure 1C-E**). Of note, during infection with *C. rodentium*, loss of GLP-1^{+} cells was transient and paralleled tissue aberration in the progressive and regressive phases of infection, with protein expression returning to basal numbers after bacterial clearance (day 32) (**Figure 1E**). Reflecting cell numbers, we observed diminished expression levels of *Gcg* (*glucagon*, translated *i.a.* into GLP-1 in the intestine) at the site of active disease in *Tnf*$^{\Delta ARE}$ mice and IL-10$^{-/-}$ mice but not unaffected tissue regions (proximal colon and distal ileum, respectively) (**Figure 1F,G**), indicating a local and acute effect of inflammatory processes on intestinal epithelial cell composition. Loss of IL-10 receptor has been shown to disrupt IEC proliferation and skew differentiation towards the goblet cell fate, implicating a role for IL-10 signaling in IEC lineage decisions (43). Yet, corroborating an inflammation-mediated over a genetic effect, we did not find any reduction in GLP-1^{+} (**Figure 1H,I**) in non-inflamed IL-10$^{-/-}$ mice on C57BL/6 background or Rag2$^{-/-}$ mice reconstituted with regulatory CD4^{+} CD25^{+} T cells, thus not developing colitis. Notably, the reconstitution of Rag2$^{-/-}$ mice with regulatory T cells did not exert any effect on GLP-1^{+} cell numbers (**Figure 1H**), suggesting lack of T cell-mediated regulation under homeostatic conditions.

For characterizing the effect of inflammation on EECs numbers in detail, we took advantage of the heterogeneity in the grade of CD-like inflammation in *Tnf*$^{\Delta ARE}$ mice and of colitis in IL-10$^{-/-}$ mice. In

independent, additional cohorts, we quantified numbers of GLP-1^{+} across a broad range of histopathological scores. Numbers of cells positive for GLP-1 inversely correlated with the grade of inflammation in the ileum of *Tnf*$^{\Delta ARE}$ mice (**Figure 1J**) and in the colon of IL-10$^{-/-}$ mice (**Figure 1K**). Comparing tissues from non-inflamed (HS <2) *Tnf*$^{\Delta ARE}$ mice and Wt C57BL/6 littermates as well as IL-10$^{-/-}$ mice and Wt 129/SvEv controls, we observed no differences in the total numbers of GLP-1^{+} (**Figure 1B,C,J,K**). Thus, loss of EECs parallels the progression towards an inflammatory tissue environment.

To confirm the human relevance of our findings, we used a recently published single-cell RNA sequencing data set from mucosal biopsies comprising healthy controls, as well as inflamed and non-inflamed tissues from CD patients (35). A total of 154,136 epithelial cells derived from terminal ileum (**Figure 1L**) and 97,788 colonic epithelial cells (**Figure 1M**), respectively, were clustered into subgroups and EECs were analyzed for *GCG* expression. In both the terminal ileum and colon, the percentage of epithelial cells expressing *GCG* dropped in the inflamed mucosa and was already altered in tissues that did not appear inflamed by endoscopic examination compared to healthy controls. Notably, also the proportion of *GCG* expressing cells among EECs was reduced, indicating GLP-1 producing cells to be particularly affected by inflammation (**Figure 1L,M**). This is in line with the data from IL-10$^{-/-}$ and *Tnf*$^{\Delta ARE}$ mice and suggests either the presence of low-grade inflammation or a persistent shift in epithelial subtype composition even in the absence of acute inflammation.

2.2 Inflammatory conditions impair epithelial differentiation into EECs

The intestinal epithelium constantly renews, and a tight balance between cell proliferation, differentiation, and apoptosis/ cell shedding is required to sustain homeostasis. Alterations in intestinal epithelial cell differentiation, subtype composition, and cell functions are part of the pathology of intestinal inflammation (15, 44). For the colonic epithelium of treatment-naïve adult CD patients, a reduction in the expression of L cell marker genes has been reported, which was linked to altered expression of transcription factors contributing to EEC maturation (44).

Thus, we performed a transcriptional analysis of isolated intestinal epithelial cells from moderately inflamed IL-10-deficient mice and Wt littermates. Expression of transcription factors involved in epithelial differentiation and marker genes of epithelial subpopulations indicate reduced terminal differentiation of epithelial cells under inflammatory conditions (**Figure 2A,B**), consistent with histologic hallmarks of inflammation including crypt hyperplasia and expansion of the transit-amplifying zone. EECs arise from the secretory linage, which also comprises antimicrobial peptide-producing Paneth cells (in the small intestine), Paneth-like cells (in the large intestine), mucin-producing goblet cells, serotonin-producing enterochromaffin cells, and tuft cells involved in chemosensing (**Figure 2B**). Secretory cells are particularly affected by inflammatory processes. For example, we found aberrant expression of the stem cell marker *Lgr5* in $Tnf^{\Delta ARE}$ mice in parallel to reduced numbers and functionality of Paneth cells (9, 39) and goblet cell-loss is a common feature of *C. rodentium*-triggered colonic inflammation (42) and colitis observed in IL-$10^{-/-}$ mice (45). Accordingly, we found an mRNA expression pattern indicating diminished presence of secretory precursor cells and reduced marker gene expression for all secretory cells except enterochromaffin cells (**Figure 2A,B**). Immunohistochemical staining and quantification of positive cells confirmed decreased numbers of Doublecortin-like kinase protein 1 $(Dclk1)^{+}$ tuft cells but stable numbers of serotonin containing $(5\text{-}HT^{+})$ enterochromaffin cell under inflammatory conditions in IL-$10^{-/-}$ mice (**Figure 2C,D**), suggesting mechanisms specifically sustaining this cell population under inflammatory conditions. In line, employing the same single-cell RNA sequencing data set (35) as before, a reduction in colonic epithelial cells expressing the mature colonocyte marker *CA1* (*Carbonic anhydrase 1*) was observed in inflamed CD patients (**Figure 2E**). At the same time, the number of colonic epithelial cells expressing the enterochromaffin cell marker *TPH1* (*Tryptophan hydroxylase1*) slightly increased in CD patients independent of the inflammatory status, resulting in an increased proportion of *TPH1*-positive cells among all enteroendocrine cells (**Figure 2E**). Of note, a tight bi-directional interaction of L cells and enterochromaffin cells has been described, with L cells expressing serotonin receptor 4

(46) and enterochromaffin cells expressing GLP-1 receptor (47). Moreover, endocrine cell differentiation is facilitated through paracrine GLP-1 and serotonin-mediated signaling involving the transcription factor neurogenin3 (Ngn3) (48). Expression of *Ngn3*, required to restrict secretory progenitors to the endocrine lineage (49) was increased in intestinal epithelial cells from inflamed IL-10$^{-/-}$ mice, together with other transcription factors of the cascade controlling terminal differentiation of enteroendocrine cell subtypes (**Figure 2A,B**). This included late acting transcription factors *Paired box gene* (*Pax*)*4*, *Pax6* and *Insulin gene enhancer protein* (*Isl*)*1*, regulating enterohormone gene transcription.

2.3 Remaining colonic L cells are functional

In particular, *Pax6* and *Isl1* directly bind consensus sequences on the *Gcg* promoter, indicating a sustained expression of *Gcg* in the reduced number of GLP-1^{+} cells in the epithelium. Following translation, proglucagon encoded by *Gcg* is cleaved into active GLP-1 by prohormone convertase (PC) 1/3 in EECs and subsequently cleaved and inactivated by dipeptidyl peptidase-4 (DPP4) in target tissues. In accordance with the hypothesis that remaining EECs sustain GLP-1 expression, expression level of *Pcsk1* (encoding PC1/3) remained unaltered under inflammation, but expression of *Dpp4* strongly decreased specifically at the site of inflammation (proximal colonic tissue) (**Figure 2F**), suggesting compensatory mechanisms to maintain GLP-1 signaling. Corroborating these results, we found reduced but substantial amounts of active GLP-1 in primary colonic crypts derived from IL-10$^{-/-}$ mice (**Figure 2G**). Furthermore, L cells remained functional as primary colonic organoids derived from IL-10$^{-/-}$ mice showed a secretory response towards stimulation with the bile acid deoxycholic acid (DCA) that did not significantly differ from that of Wt organoids (3.3 ± 0.36 *vs* 2.1 ± 0.28 fold increase), despite overall reduced secretion of GLP-1 per living cell (**Figure 2H**). Likewise indicating reduced but functional L cells, the average expression of *GCG* within colonic *GCG*$^{+}$ cells remained unaltered in the single-cell RNA sequencing data set (35) comprising healthy controls and inflamed and non-inflamed tissues from CD patients (**Figure 2I**).

2.4 Inflammatory cytokines and microbial structures affect *Gcg* expression

To investigate a potential contribution of pro-inflammatory cytokines and microbial structures to the inflammatory environment fostering L cell loss, we employed intestinal organoids derived from Wt mice. First, we tested whether microbial structures including bacterial muramyl dipeptide (MDP) and lipopolysaccharide (LPS) or the pro-inflammatory cytokines interferon γ (IFN) and TNF would induce GLP-1 secretion (**Figure 3A**). MDP is a substrate of PEPT1, known to mediate di/tripeptide-induced GLP-1 secretion in L cells and can be sensed intracellularly by nucleotide-binding oligomerization domain (NOD)-like receptors that belong to the innate immune system (50). SNPs in both *Pept1* and *Nod2* are known risk factors for IBD (51, 52). Yet, neither MDP nor treatment with a mixture of IFN/TNF led to a detectable secretion of GLP-1 despite responsiveness of organoids towards the bile acid deoxycholic acid (DCA) (**Figure 3B**). In contrast, LPS acted as a weak GLP-1 secretagogue, in accordance with literature proposing TLR4-dependent GLP-1 secretion upon LPS exposure by L cells as pathogen sensing mechanism during intestinal injury (53). A mixture of forskolin/3-isobutyl-1-methylxanthine (F/I) served as a control for maximal hormone output (**Figure 3B**).

In a second approach, organoids were stimulated with low concentrations of TNF/IFN and LPS for 48h to determine the effect on epithelial differentiation. The chosen concentrations did not impair organoid survival or growth after 48h (**Figure 3C,D**), but robustly induced Interferon gamma-induced protein 10 (IP-10) in cell lysates and supernatants after 8h (**Figure 3E,F**), indicating reactivity towards stimulation. Treatment for 48h with TNF/IFN resulted in diminished expression of *Gcg* and *Mucin 2* (*Muc2*), a marker for goblet cells, recapitulating *in vivo* inflammatory conditions (**Figure 3G**). In contrast, LPS treatment increased *Gcg* and *Muc2* expression (**Figure 3H**), which supports the hypothesis that persistent activation of L cells stimulates L cell differentiation in a paracrine manner (54) and data showing LPS-mediated upregulation of mucin expression and secretion in goblet cells (55).

2.5 Inflammation-associated impairment of mitochondrial metabolism is associated with reduced enteroendocrine cell markers

A potential mechanism by which TNF/IFN and inflammation might affect L cell numbers is by affecting cellular metabolism and particularly mitochondrial function, including oxidative phosphorylation (OXPHOS) (15, 56, 57). Previously, we established a link between impaired mitochondrial function and altered epithelial cell differentiation in the context of intestinal inflammation (9, 14, 58, 59). In particular, we found an inflammation-related metabolic fingerprint in ileal epithelial cells comprising a shift from OXPHOS to glycolysis and overall reduced cellular ATP level in *Tnf*$^{\Delta ARE}$ mice. These metabolic changes were paralleled by induction of mitochondrial stress signaling pathways and aberrances of the intestinal stem cell niche, including loss of Paneth cells (9). On the basis of these results we screened genes indicative for different inflammation-relevant cellular metabolic pathways and metabolic genes known to affect the intestinal stem cell niche (16, 59) in isolated intestinal epithelial cells from moderately inflamed IL-10-deficient mice and Wt littermates (**Figure 4A**). Reflecting previous observations, transcriptional analysis indicated holistic metabolic changes in colitis, including reduced mitochondrial metabolism, enhanced glycolysis and activation of autophagy (60). Genes involved in the dynamic metabolic adaptions required for maintaining homeostasis of the ISC niche (including *Pdk4, Sgk1, Hmgcs2* and *Mtor*) were consistently down-regulated (**Figure 4A,B**). Concomitantly, cellular ATP levels were reduced and expression of *Trib3*, a marker for activation of the mitochondrial unfolded protein response (MT-UPR), a signaling pathway related to disturbances of mitochondrial function, was enhanced (**Figure 4C,D**). Highlighting the strong link between inflammation-related epithelial metabolism and *Gcg* expression, mRNA levels of *Hk2* and *Ddit4*, genes involved in glycolysis and suppressing mammalian target of rapamycin (mTOR) activity (61, 62), negatively correlated with *Gcg* expression, while a positive correlation was observed for *Pck1* and *Hmgcs2*, genes involved in gluconeogenesis and ketogenesis, respectively (**Figure 4E**). Importantly, these finding were reflected by the single-cell RNA sequencing data set derived from

human mucosal biopsies. The frequency of colonic epithelial cells expressing marker genes for mitochondrial stress signaling (*TRIB3*, *ATF5*) and reduced cellular ATP levels (*PRKAA1* encoding the catalytic subunit of AMPK) was increased in tissues from inflamed CD patients (**Figure 4F**). Concomitantly, the proportion of colonic epithelial cells expressing metabolism-associated genes *HK2* and *DDIT4* was elevated under inflammatory conditions, while the proportion of cells expressing *PCK1* and *HMGCS2* decreased (**Figure 4G**). In line with previous results, most changes in cellular expressions were also visible in epithelial cells derived from biopsies of CD patients that were considered non-inflamed, again pointing toward cellular metabolic alterations preceding overt tissue pathology or persisting in the absence of the same. In summary, these data indicate that, consistent with ileal inflammation (9), colonic inflammatory processes are also associated with mitochondrial stress and are paralleled by reprogramming of intestinal cellular metabolism, dampening OXPHOS, and fostering glycolysis. This metabolic fingerprint accompanies the decline in GLP-1 positive cell numbers.

2.6 Mitochondrial impairment causes reduction of enteroendocrine cells

Intriguingly, deletion of the mitochondrial chaperone Hsp60 in murine colonocytes, triggering mitochondrial dysfunction and stress signaling, resembles the metabolic fingerprint of inflammation including up-regulation of *Hk2* and *Ddit4*, as well as down-regulation of *Pck1* and *Hmgcs2* (59). Elegantly demonstrating the causative contribution of metabolic disturbances to altered epithelial differentiation, this genetic model of primary mitochondrial dysfunction also shows a reduction in differentiated cells, including EECs, enterocytes, and tuft cells (but not enterochromaffin cells), as shown by single-cell RNA sequencing (59). To further establish mitochondrial impairment as a key driver of skewed epithelial differentiation processes, we used a mouse model with an epithelial-specific knockout of caseinolytic mitochondrial matrix peptidase ($ClpP^{\Delta IEC}$). ClpP contributes to mitochondrial proteostasis and knockout of ClpP triggers induction of Trib3 (63), Atf5 (64) and activation of AMPK (65). Tissue-specific ClpP deficiency in liver and skeletal muscle causes mitochondrial dysfunction

including a decrease in mitochondrial respiratory supercomplexes (64). In contrast to Hsp60, whose non-inducible IEC-specific knockout (using *Villin1*Cre transgenic mice) is embryonic lethal (58), ClpP$^{\Delta IEC}$ mice are viable and exhibit normal growth and body weight development on a standard chow diet (data not shown), indicating less severe mitochondrial impairment. Loss of ClpP was confirmed by qPCR analysis of *ClpP* mRNA in isolated IECs (**Figure 5A**). At the age of one year, morphological features of the small intestine and colon including intestinal length, number of crypts, and crypt/villus length were similar to control *ClpP*$^{flox/flox}$ littermates (**Figure 5B,C**). However, plasma concentration of citrulline, synthesized in the small intestinal epithelium as part of the urea cycle and serving as a functional readout of IEC mitochondrial function, was decreased, in line with previous results from Hsp60$^{\Delta IEC}$ mice (58) (**Figure 5D**). Additionally, Paneth cells in ClpP$^{\Delta IEC}$ exhibited reduced numbers of granules positive for the antimicrobial peptide lysozyme (Lyz^{+}) (**Figure 5E,F**). Disturbances of AMP-packaging into granules and alterations in the granule exocytosis pathway manifest as disorganized and reduced numbers of cytoplasmic granules as well as a diffuse cytoplasmic lysozyme expression(8). Therefore, morphology of Lyz^{+} secretory granules is used as a functional marker for Paneth cell phenotype classification, and both inflammation and epithelial mitochondrial dysfunction have previously been shown to correlated with reduced Paneth cell granularity (8, 9). Importantly, numbers of GLP-1^{+} cells were diminished in the ileum and proximal colon in ClpP$^{\Delta IEC}$ mice (**Figure 5G**), indicating that mild mitochondrial dysfunction in the absence of tissue aberration or overt inflammation is sufficient to compromise Paneth cell function and reduce EEC differentiation.

To further validate that disturbances of mitochondrial metabolism skew epithelial differentiation, we used the OXPHOS inhibitor oligomycin *ex vivo* in intestinal organoids. Murine intestinal Wt organoids (**Figure 5H**) and human intestinal organoids (**Figure 5I**) were treated with sub-lethal doses of oligomycin for 6h and were subsequently allowed to recover for 18h. Blockade of OXPHOS induced mitochondrial stress signaling (MT-UPR) as evidenced by *Trib3*/ *TRIB3* upregulation and led to a reduction of the enteroendocrine marker gene *Chga*/ *CHGA*, in both murine and human organoids

(**Figure 5H-I**). In summary, these data support the notion that impaired mitochondrial function in epithelial cells, as observed under inflammatory conditions, might be the driving force of reduced GLP-1^+ cell numbers.

3 Conclusion

While the mechanisms underlying hormone secretion from L cells and their functions in the context of digestion and metabolism are well studied, their role in the pathogenesis of intestinal inflammation is virtually unknown.

Quantifying GLP-1^+ cells in four mouse models of ileitis and colitis and characterizing two independent cohorts of each *Tnf*$^{\Delta ARE}$ mice and IL-$10^{-/-}$ mice, we found a consistent reduction in GLP-1 expressing cells confined to the site of active disease and correlating to the degree of inflammation. Importantly, we confirmed the reduced expression of the GLP-1-encoding gene *GCG* in a publicly available single-cell RNA sequencing data set of ileal and colonic mucosal biopsies derived from healthy controls as well as inflamed and non-inflamed tissues from CD patients (35). Hence, the loss of GLP-1^+ cells appears to be a general feature of both small and large intestinal inflammation. One major goal of this work was to give a comprehensive overview of different mouse models of intestinal inflammation and therefore, most tissue samples used were generated in the context of previous studies. This explains the lack of GLP-1 measurements in plasma, a clear limitation that has to be overcome in subsequent studies. However, previous data do not indicate a reduced glucose tolerance in IL-10 deficient mice (60). This could be attributed to location-specific functions that have been proposed for GLP-1, with ileal GLP-1 stimulating insulin release in response to nutrients (66) and colonic GLP-1 exerting rather local effects, *i.e.*, slowing gastrointestinal transit time (67). Furthermore, total changes in hormone secretion depend on the severity of inflammation and the extent of tissue affected and thus, might be too minor to be recovered systemically. Especially when considering the heterogeneity of IBD pathologies, this could contribute to inconsistent data for IBD patients (27). Nevertheless,

paracrine signalling of GLP-1 might have profound effects on enterochromaffin cells (47), intraepithelial lymphocytes (29) and afferent neurons, in turn impacting intestinal motility, mucosal immune responses and feeding patterns, respectively.

EECs sense the luminal and lamina propria environment, not only reacting to bacterial structures like LPS through pattern recognition receptors (66, 68, 69), and bacterial metabolites such as SCFA and indole (70), but also express TNF receptor 1 (71). In addition to GLP-1 release, exposure to flagellin or lipopolysaccharide (72, 73) also results in expression of pro-inflammatory cytokines and evokes a gene response indicating EECs to participate in innate immune responses to commensals and pathogens (72). The observations led to the suggestion of an immunoendocrine axis and a critical role for EECs in orchestrating an intestinal metabolic-inflammatory response (74, 75), a mechanism most likely of relevance to IBD.

Hormone expression patterns of L cells differ considerably depending on their location in the intestine (76-78) and technical advances made the one cell-one hormone dogma obsolete (79, 80). GLP-1 is co-expressed with GLP-2, peptide YY (PYY), glucose-dependent insulinotropic polypeptide GIP, cholecystokinin (CCK) and secretin. Thus, the reduction of GLP-1 expressing cells under inflammatory conditions in the intestine should also profoundly affect signaling of additional gut hormones, and indeed, next to *GCG*, also *PYY* was found to be diminished in colonic epithelial cells from treatment-naïve adult CD patients (44). With regard to mucosal homeostasis, GLP-2, posttranslationally processed from proglucagon like GLP-1 and secreted in equimolar amounts (81), is of particular interest. GLP-2 is an epithelial growth factor implicated in tissue healing following injury, improving barrier function and restoring epithelial homeostasis. Furthermore, GLP-2 possesses anti-inflammatory properties and sustains Paneth cell function (82). Consequently, it has been shown to ameliorate experimental colitis in several animal models (83-86) and a GLP-2 analog was proven effective in the treatment of active moderate to severe CD (87).

Importantly, we link the loss of GLP-1^{+} cells to an inflammation-related epithelial metabolic signature that was previously associated with impaired Paneth cell and goblet cell differentiation (9, 14) and that is reflected in colonic epithelial cells of CD patients. In accordance with the pivotal role of mitochondria in steering differentiation processes by balancing OXPHOS and glycolysis, compromised mitochondrial function in ClpP$^{\Delta IEC}$ mice, as well as *ex vivo* inhibition of OXPHOS in organoid cultures, was sufficient to impair EEC development.

This is in line with previous data (9, 88) and points toward compromised mitochondrial function as underlying cause of altered epithelial cell composition during the onset of inflammatory processes. Underlining the translatability of findings to the human disease condition, a downregulation of the ketogenesis pathway, as expected by a drop in *HMGCS2* expression, has been described for colonocytes of CD patients (35) and in line, reduced levels of the ketone body β-hydroxybutyrate were observed in the colonic mucosa of IBD patients which correlated with IBD activity index (89). Of note, a similar pattern of *HK2* expression to that we found in the single-cell RNA sequencing data set of CD patients (lowest in healthy controls and gradual increase from non-inflamed to inflamed tissue samples from IBD patients) has recently been reported in another cohort of IBD patients (90).

Remarkably, analysis of the single-cell RNA sequencing data set CD patients revealed metabolic changes and signs of mitochondrial stress signaling as well as changes in epithelial subtype composition even in mucosal tissues that were considered non-inflamed by endoscopy. Considering the chronic remittent pathology of CD with phases of remission and flares of inflammation, these cellular metabolic changes might render the mucosa susceptible for additional inflammatory triggers.

Consequently, improving metabolic fitness and metabolic reprogramming have been identified as new therapeutic targets combating IBD by restoring functionality of IEC subtypes and enforcement of the epithelial regenerative capacity (14). Although so far rather neglected as player in intestinal inflammation, EECs might also profit from such metabolic interventions.

Recently, the influence of GLP-1 receptor agonists on the disease course of CD and UC patients with concomitant type 2 diabetes was investigated in a large-scale cohort study. The results suggest a potential therapeutic advantage of GLP-1 receptor agonists in managing IBD, by reducing hospitalizations, surgeries, and mortality (91). These beneficial outcomes underline the need for more research to scrutinize the role of GLP-1 in the pathogenesis of intestinal inflammation. However, given the numerous properties of GLP-1, it is likely that it affects inflammatory processes in the mucosa and disease-related symptoms on multiple levels (**Figure 6**). Thus, EECs and GLP-1-based therapies could represent an independent, promising strategy for intestinal inflammatory diseases.

4 Figures + Legends

4.1 Figure 1: GLP-1^{+} cells are reduced in the murine and human intestinal mucosa under inflammatory conditions

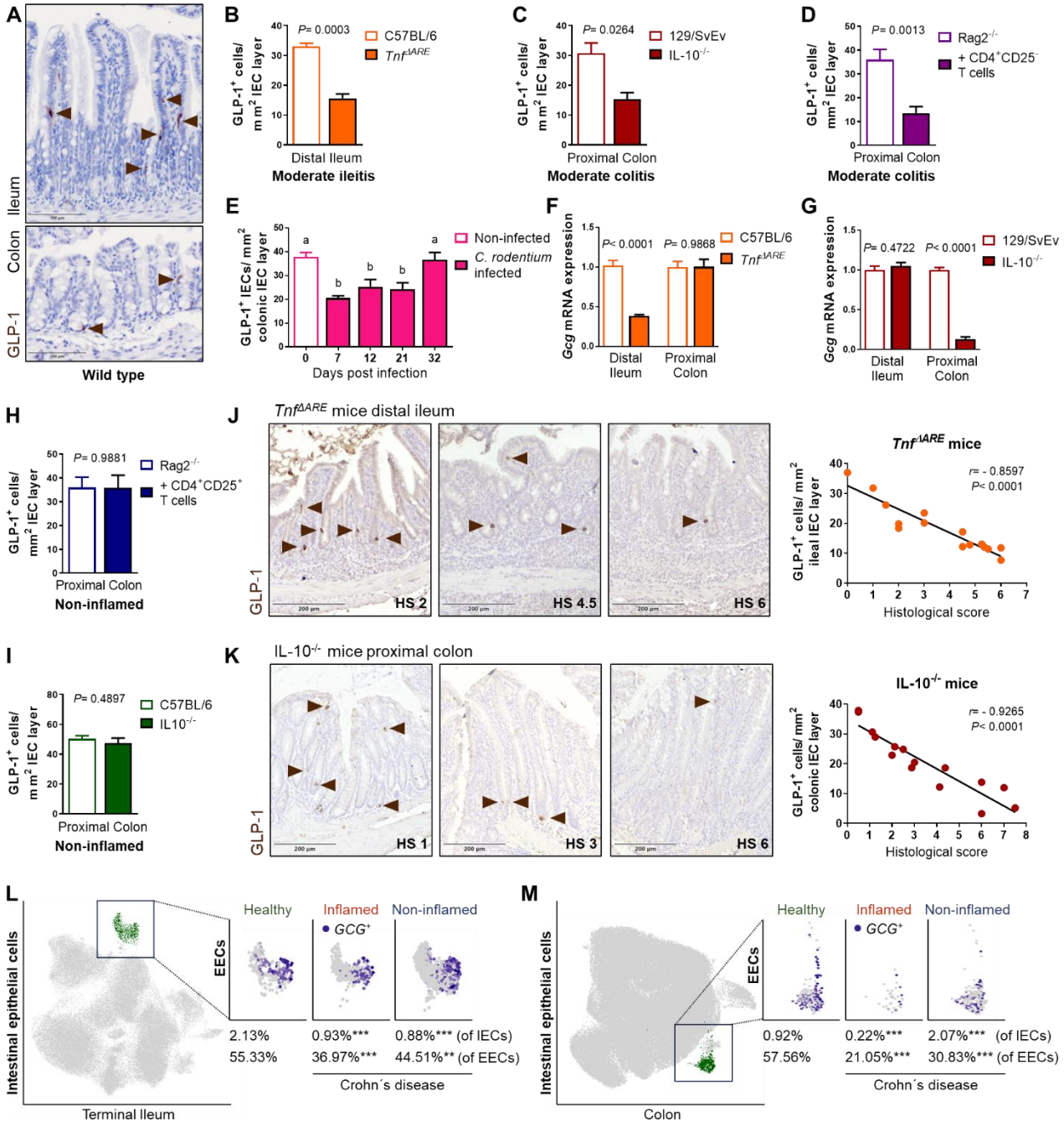

(**A**) Representative pictures of ileal and colonic tissue sections from wild type mice immunohistochemically (IHC) stained for GLP-1. Arrows indicate cells positive for GLP1. (**B-D**)

Quantification of GLP-1-positive cells (**B**) in ileal tissue sections of moderately inflamed (histological score (HS) 2-4) *Tnf*$^{\Delta ARE}$ mice, (**C**) in colonic tissue sections of moderately inflamed IL-10$^{-/-}$ mice, (**D**) in colonic tissue sections of moderately inflamed Rag2$^{-/-}$ mice adoptively transferred with colitogenic CD4^{+} CD25^{-} T cells, and respective controls. (**E**) Quantification of GLP-1-positive cells in colonic tissue sections of mice infected with *Citrobacter (C.) rodentium* prior to and at different time points post infection. (**F, G**) qRT-PCR analysis for *Gcg* (encoding GLP-1) of ileal and colonic tissue from (**F**) *Tnf*$^{\Delta ARE}$ mice and (**G**) from IL-10$^{-/-}$ mice including respective controls. Expression levels are normalized to controls and tissue of origin. (**H,I**) Quantification of GLP-1-positive cells in colonic tissue sections (**H**) of non-inflamed Rag2$^{-/-}$ mice adoptively transferred with regulatory CD4^{+} CD25^{+} T cells and (**I**) of non-inflamed IL-10$^{-/-}$ mice on C57BL/6 background and respective controls. (**J,K**) Representative GLP-1 IHC stainings for the HS indicated (left) and correlation analysis (Pearson) of the number of GLP-1-positive cells and HS for (**J**) ileal tissue from *Tnf*$^{\Delta ARE}$ mice and (**K**) colonic tissue from IL-10$^{-/-}$ mice. (**L**, **M**) Uniform manifold approximation and projection (UMAP) visualization of scRNA-sequencing of intestinal epithelial cells from the terminal ileum (**L**) and colon (**M**) from Crohn´s disease patients (35). The subgroup of enteroendocrine cells is highlighted in green (left) and *GCG*-expressing enteroendocrine cells are shown in purple in healthy, inflamed and non-inflamed conditions (right). The sample size for healthy/ inflamed/ non-inflamed is 11/ 14/ 45 for (**L**) and 32/ 5/ 18 for (**M**), respectively. Chi-square test and Fisher´s exact test, asterisks indicate differences compared to healthy controls, **P*<0.05, ***P*<0.01, ****P*<0.001. (**B-I**) Bars represent mean+SEM, n≥5 for all groups. Unpaired t tests except (**E**) one-way ANOVA followed by Tukey test. *P* values and r are indicated; a is significantly ($P < 0.05$) different from b.

4.2 Figure2: Inflammation selectively impairs epithelial differentiation but not L cell function

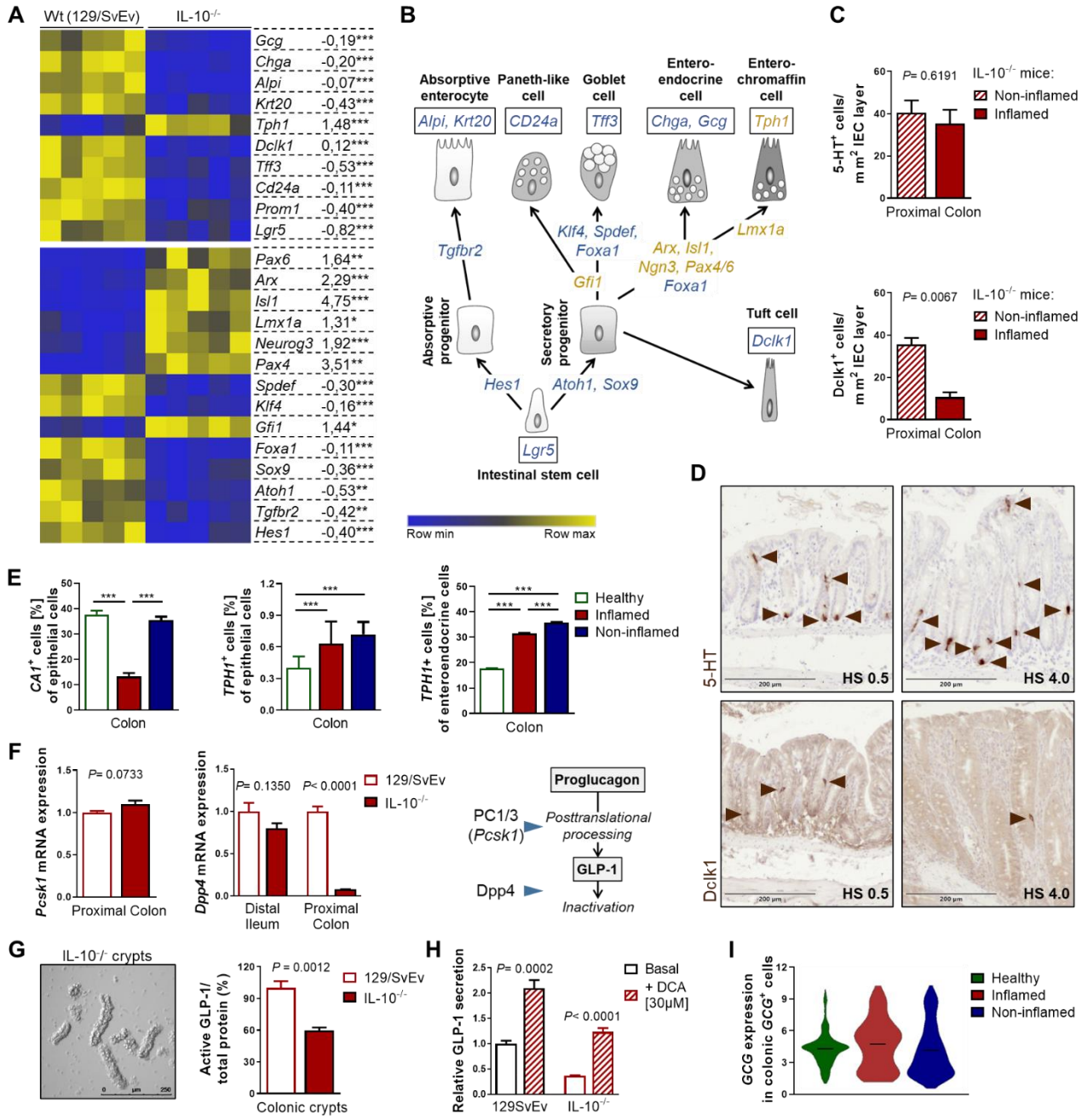

(**A**) Heatmap of a transcriptional profile of isolated intestinal epithelial cells from moderately inflamed (histological score (HS) 2-4) IL-10$^{-/-}$ mice and wild-type (Wt) controls showing marker genes for epithelial subtypes and genes involved in epithelial differentiation. Fold changes in gene expression are given on the right side. Asterisks indicate significant differences **P*<0.05, ***P*<0.01, ****P*<0.001. (**B**) Schematic representation of marker gene expression during differentiation and in epithelial

subtypes. Blue = down-regulation, yellow = up-regulation under inflammatory conditions. (**C**) Quantification of 5-HT (serotonin)-positive enterochromaffin cells and Dclk1-positive tuft cells in colonic tissue sections of non-inflamed and inflamed IL-10$^{-/-}$ mice. (**D**) Representative 5-HT and Dclk1 IHC stainings for the HS indicated. Arrows indicate cells positive for the respective marker. (**E**) Barplots showing the proportion of epithelial cells expressing *CA1*, a marker gene of mature colonocytes, (left) and *TPH1*, encoding the enzyme required of 5-HT generation, (middle) and *TPH1* expression within enteroendocrine cells (right) in a scRNA-sequencing dataset of colonic intestinal epithelial cells from Crohn´s disease patients (35). One-way ANOVA followed by Tukey test, asterisks indicate significant differences *P<0.05, **P<0.01, ***P<0.001. (**F**) qRT-PCR analysis for *Pcsk1* and *Dpp4*, enzymes regulating GLP-1 abundance (right), of ileal and colonic tissue from IL-10$^{-/-}$ mice and wild-type (Wt) controls. (**G**) Representative picture of isolated colonic crypts from inflamed IL-10$^{-/-}$ mice (left). Quantification of active GLP-1 (ELISA) in isolated colonic crypts from moderately inflamed IL-10$^{-/-}$ mice and Wt controls (right). (**H**) Basal and deoxycholic acid (DCA)-induced secretion of active GLP-1 from primary colonic organoids derived from IL-10$^{-/-}$ mice and Wt controls. Basal secretion from Wt colonic organoids is set as “1”. Bars represent mean+SEM, n≥5 for all groups. Unpaired t tests, P values and are indicated. (**I**) Violin plot from the same dataset as in (**E**) showing the normalized expression height and distribution of *GCG* within *GCG*-expressing colonic epithelial cells. No significant differences are observed (one-way ANOVA).

4.3 Figure 3: Inflammatory stimuli and microbial structures differentially affect *Gcg* gene expression and GLP-1 secretion

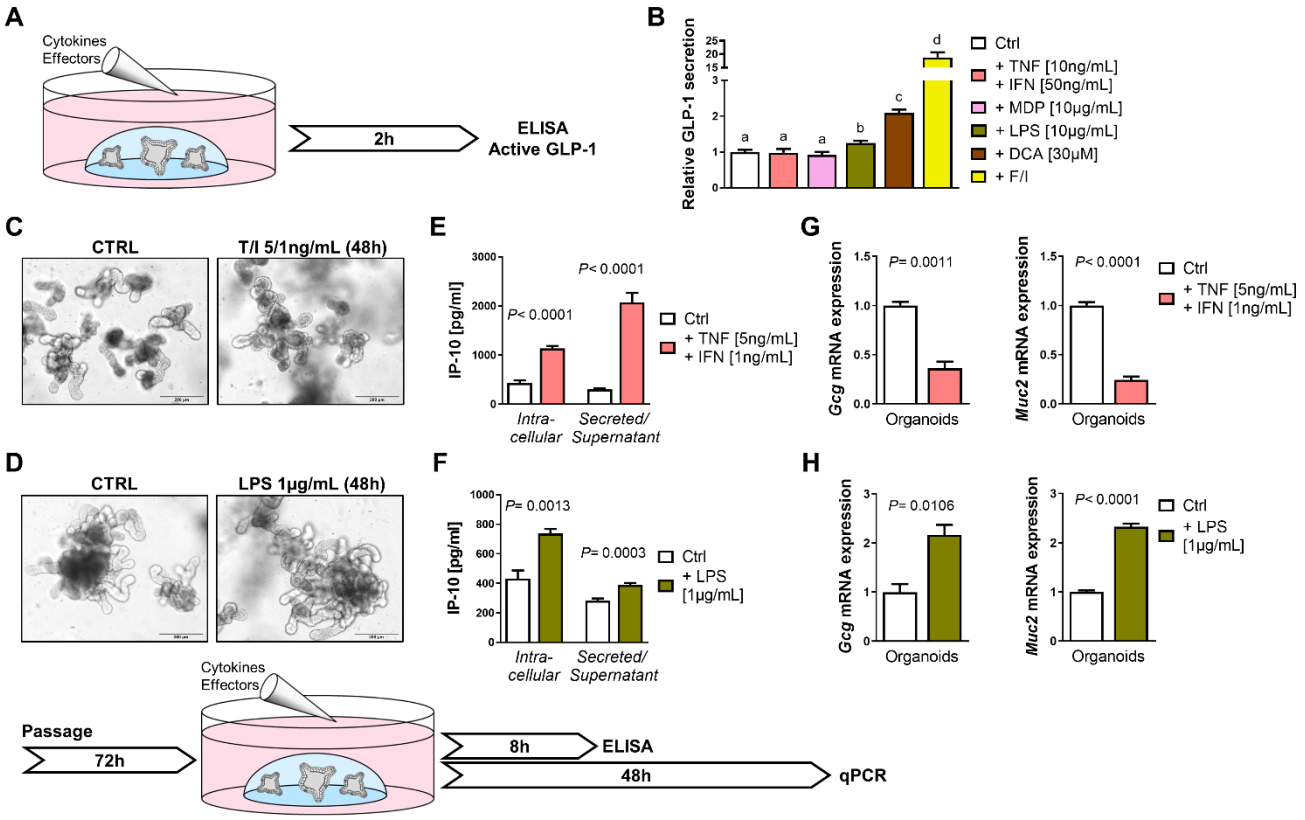

(**A**) Schematic representation of the experimental setup for (**B**), secretion of active GLP-1 (ELISA) from wild-type (Wt) intestinal organoids stimulated with bacterial-derived Lipopolysaccharide (LPS) or Muramyl dipeptide (MDP), or pro-inflammatory cytokines tumor necrosis factor (TNF) and Interferon gamma (IFN), respectively. Deoxycholic acid (DCA) serves as physiological positive control, forskolin/3-isobutyl-1-methylxanthine (F/I) induces maximal secretion. (**C,D**) Representative pictures of Wt intestinal organoids stimulated with TNF/IFN (**C**) or LPS (**D**) showing no growth impairment and schematic representation of the experimental setup. (**E,F**) Intracellular protein levels and secretion of the pro- inflammatory cytokine IP-10 in Wt intestinal organoids stimulated with (**E**) TNF/IFN or (**F**) LPS, respectively. (**G,H**) qRT-PCR analysis for *Gcg* and *Muc2* of intestinal organoids stimulated with (**G**) TNF/IFN or (**H**) LPS, respectively. (**B, E-H**) Bars represent mean+SEM, n≥5 for

all groups. Unpaired t tests except (**B**) one-way ANOVA followed by Tukey test. *P* values are indicated; a, b, c, d are significantly ($P < 0.05$) different from each other.

4.4 Figure 4: The inflammation-related metabolic profile is associated with GLP-1^{+} cell loss

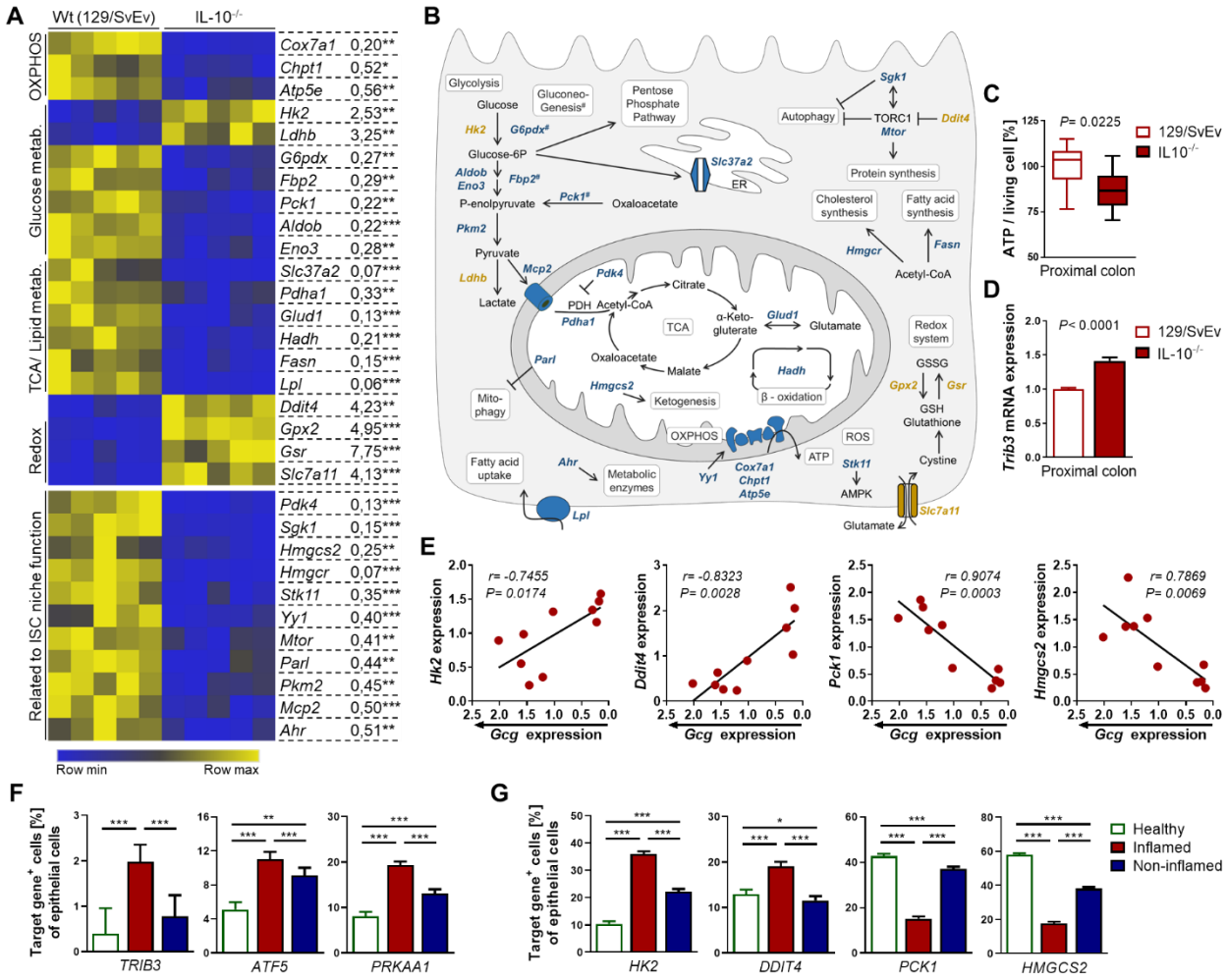

(**A**) Heatmap of a transcriptional profile of isolated intestinal epithelial cells from moderately inflamed (HS 2-4) IL-10$^{-/-}$ mice and wild-type (Wt) controls showing metabolism-associated genes involved in different metabolic processes and stem cell niche function. Fold changes in gene expression are given on the right side. Asterisks indicate significant differences *P<0.05, **P<0.01, ***P<0.001. (**B**) Schematic representation of metabolic gene functions. Blue = down-regulation, yellow = up-regulation under inflammatory conditions. (**C**) ATP content of primary isolated colonic crypts from IL-10$^{-/-}$ mice and Wt controls. (**D**) qRT-PCR analysis of isolated colonic epithelial cells for *Trib3*, a marker gene for mitochondrial stress signaling. (**E**) Correlation (Pearson) of metabolic gene expression with *Gcg* mRNA level in colonic epithelial cells isolated from IL-10$^{-/-}$ mice. (**F, G**) Barplots showing the

proportion of colonic epithelial cells expressing marker genes for mitochondrial stress signaling (*TRIB3*, *ATF5*) and AMP kinase activation (*PRKAA1*) or (**G**) target metabolic genes in a scRNA-sequencing dataset of colonic intestinal epithelial cells from Crohn´s disease patients (35) and SD of expression. One-way ANOVA followed by Tukey test, asterisks indicate significant differences *$P<0.05$, **$P<0.01$, ***$P<0.001$.

4.5 Figure 5: Mitochondrial dysfunction impairs epithelial differentiation into L cells

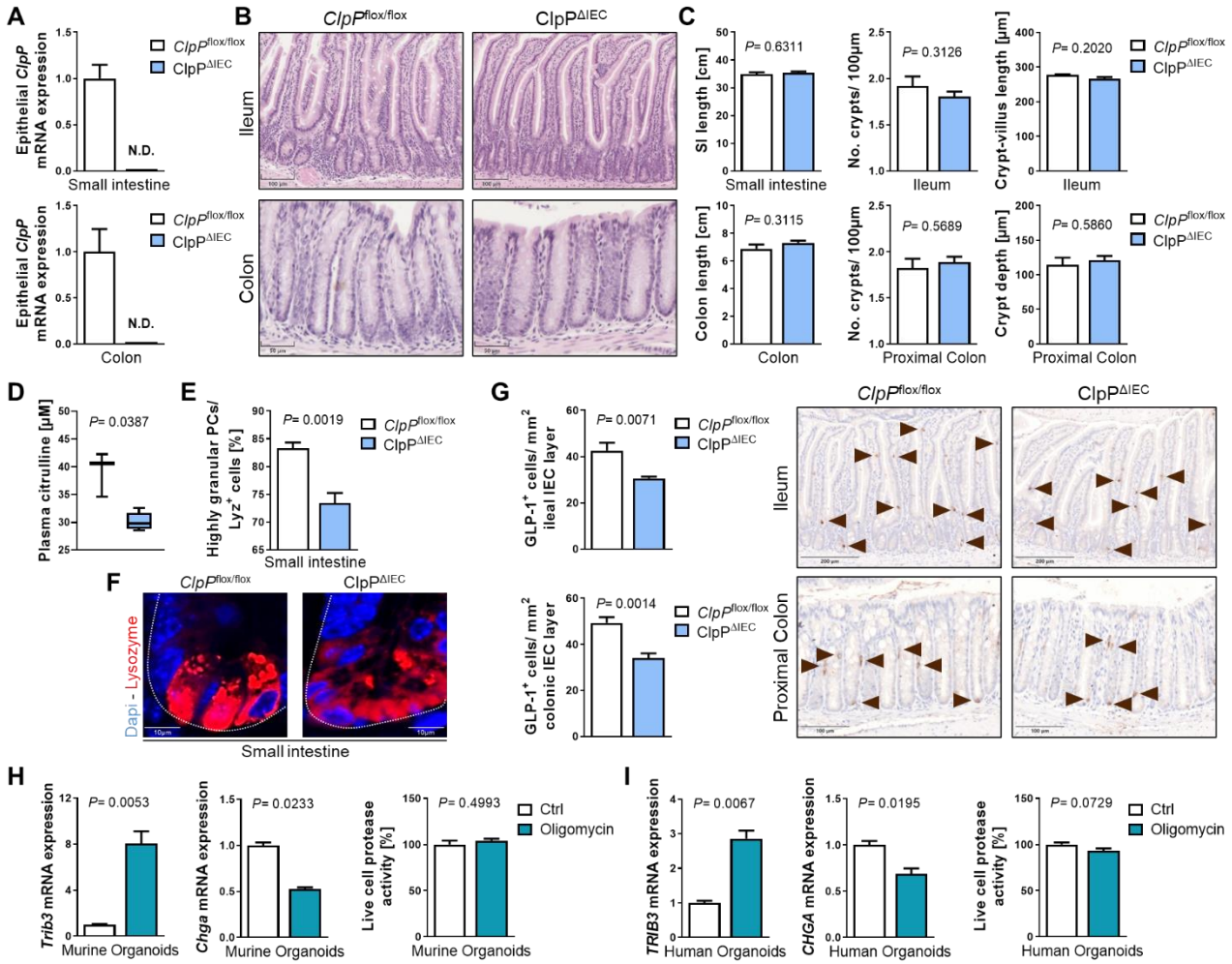

(**A**) qRT-PCR analysis for *ClpP* in small intestinal and colonic IECs from ClpP$^{\Delta IEC}$ mice and control *ClpP*$^{flox/flox}$ littermates. (**B**) Representative pictures of ileal and colonic tissue sections, (**C**) intestinal morphologic features and (**D**) Plasma citrulline level of ClpP$^{\Delta IEC}$ mice and controls. (**E**) Quantification of highly granular Lyz^{+} Paneth cells (PC) (≥2 granules) and (**F**) representative immunofluorescence staining of Lysozyme (red) counterstained with Dapi (nuclei, blue) in ClpP$^{\Delta IEC}$ mice and controls. (**G**) Quantification of GLP-1-positive cells and representative pictures of ileal and colonic tissue sections from ClpP$^{\Delta IEC}$ mice and controls immunohistochemically stained for GLP-1. Arrows indicate cells positive for GLP1. (**H**) qRT-PCR analysis of murine intestinal organoids treated with oligomycin (for 6h followed by 18h recovery) for *Trib3* and the enteroendocrine cell marker Chga. *Right*: measurement

of living cells in organoid cultures after oligomycin treatment. (**I**) Same analysis as in (**H**) for human organoids. Bars represent mean+SEM, n≥5 for all groups. Unpaired t tests, *P* values and are indicated.

4.6 Figure 6: Schematic representation of GLP-1 functions, inflammation-associated epithelial alterations and IBD symptoms.

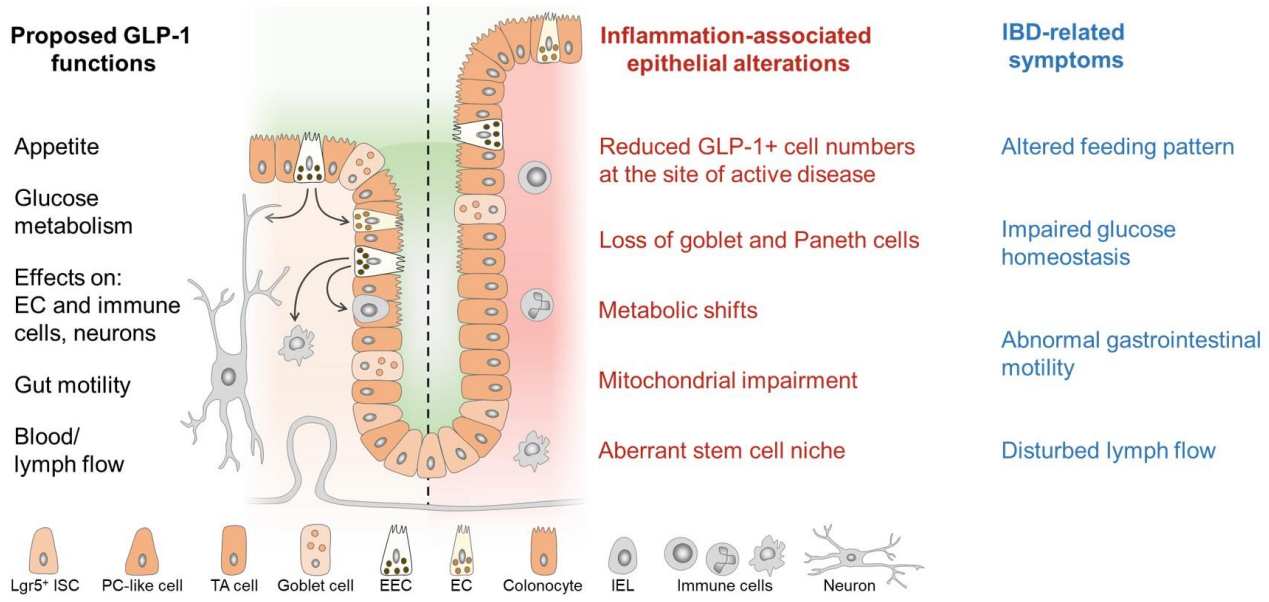

Schematic representation of GLP-1 functions, inflammation-associated epithelial alterations and IBD symptoms.

5 Methods

5.1 Ethics statement

The maintenance and breeding of mouse lines and all experiments were approved by the Institutional Animal Care and Use Committee (IACUC), University of North Carolina at Chapel Hill, NC or approved by the Committee on Animal Health and Care of the local government body of the state of Upper Bavaria (Regierung von Oberbayern; approval numbers 55.2-1-54-2531-164-09, 55.2-1-54-2531-99-13, 55.2-1-54-2532-217-2014) and performed in strict compliance with the EEC recommendations for the care and use of Lab. Anim. (European Communities Council Directive of 24 November 1986 (86/609/EEC)). For generation of human organoids, the use of surgically resected human tissue samples was approved by the Ethics Committee of the Medical Faculty of TUM and all participants in this study gave their written informed consent.

5.2 Animals

In accordance with 3R principles, most samples analyzed in this study for IHC-based quantification of intestinal cells were obtained from our tissue biobank and generated in the context of previously published studies (9, 36-38, 92).

IL-10-deficient (IL-10$^{-/-}$) mice on 129Sv/Ev background or C57BL/6 background, ***Tnf$^{\Delta ARE}$*** **mice** and **ClpP$^{\Delta IEC}$ mice** were housed (12h light/ dark cycles, 24-26˚C) under specific pathogen-free (SPF) conditions according to the criteria of the Federation for Laboratory Animal Science Associations (FELASA) and bred for several generations in the animal facility. *Tnf$^{\Delta ARE}$* mice were initially provided from Case Western University, Cleveland. *ClpP*$^{flox/flox}$ mice were generated by Taconic-Artemis (Cologne, Germany) in close consultation with our lab, similar to described previously by others(93). To generate epithelial cell-specific ClpP knockout (ClpP$^{\Delta IEC}$) mice, *ClpP*$^{flox/flox}$ mice were crossed to Cre transgenic *Villin1*Cre mice (C57Bl/6N), originally provided by Klaus-Peter Janssen (Klinikum

Rechts der Isar, TU München). Mice received a standard chow diet (autoclaved V1124-300; Ssniff, Soest, Germany) and autoclaved water ad libitum. IL-10$^{-/-}$ mice, *Tnf*$^{\Delta ARE}$ mice and Wt littermates were sacrificed at 16-18 weeks of age (9, 36, 37). Male ClpP$^{\Delta IEC}$ mice were analyzed at one year of age. Animals were killed by CO_2 inhalation.

Adoptive T -cell transfer experiments were performed as previously described (38, 92). Briefly, lymphocyte-deficient SPF 129 SvEv recombination-activating gene (Rag) 2$^{-/-}$ mice were reconstituted at 8 weeks of age by intraperitoneal injection of 5 x 10^5 CD4$^+$ T cells. CD4$^+$ CD25$^-$ and CD4$^+$ CD25$^+$ T cells for transfer were obtained from splenocyte suspensions of SPF Wild type mice using a magnetic bead-based CD4$^+$ T cell-isolation kit or the CD4$^+$ CD25$^+$-Regulatory T cell-isolation Kit (Miltenyi Biotec) according to the manufacturer's instructions. 4 weeks later, mice were killed by CO_2 anesthesia followed by cervical dislocation. Reconstitution of mice was confirmed by flow cytometric analysis. Non-reconstituted Rag2$^{-/-}$ mice served as controls.

***Citrobacter rodentium* infection**. The *C. rodentium* strain DBS100 (ATCC 51459; American Type Culture Collection) was used for infection as previously described (94). *C. rodentium* was grown overnight at 37°C in Luria broth. C57BL/6J mice were infected by oral gavage with 0.5 mL of phosphate-buffered saline (PBS) containing approximately 1×10^9 CFU of C. rodentium. To assess the clearance of C. rodentium, fecal pellets were collected from individual mice, homogenized in PBS, serially diluted and plated onto selective MacConkey agar. After an overnight incubation at 37°C, colonies were counted based on the size and distinctive appearance of *C. rodentium* colonies.

5.3 Mouse tissue processing and histopathological analysis

The intestine was removed immediately after euthanization, trimmed free of adjacent tissue and cleaned of stool. Ileal or proximal colonic intestinal tissue was either immediately fixed for preparation of cross sections or cut open and processed as 'swiss role'. Tissues were fixed in 4% phosphate-buffered

formalin for 48h, dehydrated and embedded in paraffin (FFPE). For histopathological assessment, 5 µm sections were stained with hematoxylin (of Mayer) and 0.2% eosin (ethanolic solution; both Medite) in an automated staining machine (Leica). Images were acquired by a PreciPoint M8 microscope (Precipoint). Ileal and colonic sections were blindly assessed for mononuclear cell infiltration into lamina propria, crypt hyperplasia, goblet cell depletion and ulcer formation resulting in a score from 0 (not inflamed) to 12 (highly inflamed) as described previously (45).

5.4 **Immunohistochemistry**

Immunohistochemical (IHC) stainings were performed on 5 µm FFPE tissue sections as described previously (58). Briefly, FFPE tissue sections were deparaffinized and rehydrated in an automated staining machine (Leica). After heat-mediated antigen retrieval (boiling in 10mM citrate buffer (pH=6) in a microwave (23min; 900 watt)), sections were incubated for 10min with 3% H_20_2 (Sigma-Aldrich). Subsequently, sections were blocked, and a primary antibody was applied overnight at 4°C. After several washing steps, sections were incubated with the secondary antibody (horseradish peroxidase coupled; 1h, room temperature). Antigen detection was performed using 3,3′-diaminobenzidine (DAB) or enhanced DAB (Sigma Aldrich), and nuclei were counterstained with hematoxylin. Slides were mounted with xylol-based mounting medium (Roti®-Histokitt). Stainings were scanned and using a PreciPoint M8 microscope (Precipoint). Antibodies and dilutions are given in **Table 1 and 2**.

5.5 **Immunofluorescence and Paneth cell phenotype quantification**

Immunofluorescence stainings for lysozyme were performed on 4 µm FFPE tissue sections as described previously(9). Antibodies used were: Anti-Lysozyme Rabbit Dako, Agilent, Santa Clara (1:1000), Alexa Fluor donkey anti rabbit 546 Life Technologies, Carlsbad, CA (1:200) and Dapi to counterstain nuclei, Sigma- Aldrich, Taufkirchen, Germany (1:1000). Stainings were visualized using the Flouview FV10i microscope (Olympus, Shinjuku, Japan). Lysozyme positive cells numbers were

determined in ileal tissue sections. A total number of 50 (for mice) well oriented crypts were quantified. To assess the granularity of Lyz positive cells, all PCs contained in 50 crypts were analyzed. Lyz positive cells were considered as highly granular if ≥2 Lyz positive granules were visible within the cell. The quantification was performed in a blinded manner.

5.6 Quantification of cell numbers

At least three non-consecutive sections from each mouse were used for quantification of GLP-1, ChgA or 5-HT positive cells. Well-oriented (visible open crypts/ crypt-villus axis) tissue areas were selected and epithelial cells positive for the respective marker were counted. The number of positive cells was calculated over the total epithelial area quantified using the ViewPoint Light software (Precipoint). For individual mice, the number of positive cells was calculated as mean of quantified sections and areas. The quantification was performed in a blinded manner.

5.7 Isolation of primary IECs

Primary IECs were purified as previously described (58). Approximately 6 cm of intestine were inverted on a needle, vortexed vigorously and incubated (37 °C, 15 min) in DMEM containing 10% fetal calf serum (Biochrom), 1.0% Glutamine, 0.8% antibiotics/antimycotics (all Sigma-Aldrich) supplemented with 1 mM dithiothreitol (Roth). The IEC suspension was centrifuged (7 min, 300*g*, RT) and the cell pellet was re-suspended in DMEM containing fetal calf serum, l-glutamine and antibiotics. The remaining tissue was incubated in 20 ml PBS (10 min, 37 °C) containing 1.5 mM EDTA (Roth). After vortexing, the tissue was discarded and the cell suspension from this step was centrifuged as mentioned above. Cells obtained in both steps were combined and primary IECs were purified by centrifugation through a 20%/40% discontinuous Percoll gradient (GE Healthcare) at 600*g* for 30 min. IECs were immediately snap frozen.

5.8 Primary crypt isolation and intestinal organoid culture

Primary intestinal crypts from mouse (ileum, colon) and human (from macroscopically healthy tissue of surgical specimen of the ileum) were isolated by tissue incubation in 2mM EDTA (Fisher) or Gentle Cell Dissociation Reagent (STEMCELL Technologies), respectively, and cultured as described elsewhere (58, 95, 96). For organoid culture, murine crypts were embedded in 25µl matrigel (BD Biosciences) and cultured in 48 well plates. Murine organoids were grown in crypt culture medium (CCM), advanced DMEM/F12 medium (Gibbco) containing 2 mM GlutaMax (Gibbco), 10 mM HEPES, penicillin, streptomycin and amphotericin (all Sigma- Aldrich) supplemented with N2, B27 (both Gibbco), 1 mM N-acetylcystein (Sigma- Aldrich), 50 µg/mL EGF (ImmunoTools), 100 µg/mL noggin and 0.5 µg/mL R-spondin 1 (both PeproTec) or, when derived from colonic crypts, in Murine Intesticult medium (STEMCELL Technologies). For human organoid culture, 500 crypts were embedded in 30µl matrigel (BD Biosciences) per well, resulting in approx. 100 mature organoids, and cultured in 48 well plates. Human organoids were cultivated in Human Intesticult medium (STEMCELL Technologies) containing Wnt factors.

5.9 **Intestinal organoid stimulation**

For assessing the GLP-1 secretory capacity of IL-10$^{-/-}$ enteroendocrine cells, primary colonic crypts were embedded in matrigel and cultured for 48h prior to stimulation to retain the inflammatory phenotype. For other experiments, murine and human organoids were used 4 to 6 days after passaging. Two days prior to the start of experiments, medium of human organoids was changed to CCM to reduce stem niche factors (96). When indicated, organoids were stimulated with TNF (5ng/mL) and IFN (1 ng/mL) or LPS (1µg/mL) for 48h, or treated with 2.5µM oligomycin (Sigma- Aldrich) for 6h and subsequently cultured in CCM for 18h, for gene expression analysis to assess differentiation. To measure IP-10 production and secretion, organoids were stimulated with TNF/ IFN or LPS in the same concentrations for 24h. To measure GLP-1 secretion, organoids were washed four times with HEPES-saline buffer (pH 7.4) containing BSA and DPP4 inhibitor. Subsequently, organoids were incubated

for 2h in HEPES-saline buffer supplemented with either LPS (10µg/mL), MDP (10µg/mL), a combination of TNF (10ng/mL) and IFN (50 ng/mL), DCA (30 µM) (as physiological positive control), or a mixture of 10 µM Forskolin and 10 µM 3-isobutyl-1-methylxanthine (F/I, for maximal hormone output).

5.10 **GLP-1 measurements**

Organoid culture: after stimulation, the culture plate was placed on ice, supernatants were collected and immediately cold PBS was added to the organoid cultures. Supernatant samples were centrifuged (400 g) for 5 min at 4 °C and the supernatant was snap-frozen in liquid nitrogen. Organoids including Matrigel were resuspended in cold PBS and washed twice by centrifugation (600 g) for 10 min at 4 °C. The organoid pellet was dissolved in lysis buffer containing 150 mM NaCl, 50 mM Tris-HCl, 1% Igepal CA-630, 0.5% DCA and a protease inhibitor mix, for 20 min at 37 °C, and centrifuged (600 g) for 10 min at 4 °C. The supernatant was collected and snap-frozen. Primary crypts were lysed and processed accordingly. All samples were kept at −80 °C until analysis of incretin hormones. GLP-1 concentrations in supernatant and lysate were quantified using a Glucagon-Like Peptide 1 (Active) ELISA kit (Millipore). The amount of GLP-1 secreted by the cultures was calculated as a percentage of the GLP-1 content (secreted plus intracellular) and normalized to basal secretion. The content of active GLP-1 in primary crypts was normalized to total protein content (determined by Bradford assay) of samples and calculated as percentage of Wt (129/SvEv) colonic crypts.

5.11 **IP-10 measurements**

After stimulation, supernatants and organoids were collected according to the procedures described for GLP-1 measurement. The organoids were dissolved using a non-denaturating lysis buffer containing PMSF and a protease inhibitor mix. IP-10 concentrations were determined using an IP-10 ELISA kit (R&D Systems) according to the manufacturer’s instructions.

5.12 Measurement of living cells and cellular ATP content

Life- and dead- cell protease activity was measured using the MultiTox-Fluor Cytotoxicity Assay and ATP content was determined using the CellTiter-Glo Luminescent Cell Viability Assay (both from Promega), according to the manufacturer's instructions. Fluorescence and luminescence were measured using the Tecan infinite M200 (Tecan Group Ltd.) and the i-control™ Microplate Reader software (Tecan).

5.13 Measurement of plasma citrulline

EDTA blood was taken during sampling from venacava. Quantitation of amino acids in EDTA plasma was performed using LC–MS/MS with aTRAQ labelling (aTRAQ reagent kit 4442671, AB SCIEX, Framingham, MA, USA). Quantitation was done according to the manufacturer's instructions using 40 µl of serum sample. The analysis was performed on a triple quadrupole QTRAP3200 LC–MS/MS system (AB SCIEX) coupled to an Agilent 1260 Infinity Quaternary LC Pump (Agilent, Santa Clara, CA, USA).

5.14 RNA isolation, reverse transcription and quantitative real-time PCR

For mRNA isolation from primary IEC or organoids, the NucleoSpin RNAII kit (Macherey-Nagel) was used according to the manufacturer's instructions. In the case of organoid culture, matrigel containing organoids was directly dissolved in RA1 buffer. Reverse transcription was performed as previously described (97). Quantitative Real-time PCR (qRT–PCR) was performed using the Light Cycler 480 system (Roche Diagnostics) and applying the Universal Probe Library system according to the manufacturer's instructions. Primer sequences and probes are given in **Table 3**. Relative induction of gene mRNA expression was calculated based on Ct values using the expression of house-keeping genes *HPRT*/*Hprt* for normalization. Data are expressed as fold change over controls.

5.15 Single-cell RNA sequencing and data visualization

The single-cell RNA sequencing dataset comprising intestinal epithelial cells from the terminal ileum and colon of healthy donors as well as inflamed and non-inflamed tissues from Crohn´s disease patients was obtained from https://explore.data.humancellatlas.org/projects/cae461de-ecbd-482f-a5d4-11d607fc12ba and initially published by Kong et al. (35). Data from 720,633 cells across 71 donors with various inflammation statuses were processed in R (v4.3.3) using Seurat (v5.1.0). Gene symbols were mapped from Ensembl IDs with biomaRt (v2.58.2). UMAP plots were generated to highlight GCG-positive cells, and a subset of enteroendocrine cells was created. The proportion of GCG-expressing cells, as well as cells positive for mitochondrial stress markers and selected metabolic genes, was calculated within subsets, and mean expression levels of genes were computed by inflammation status (healthy, inflamed, and non-inflamed), including standard deviation, sample size, and standard error of the mean.

5.16 Statistical analysis and heatmap generation

Heatmaps were generated using Morpheus (https://software.broadinstitute.org/morpheus). Statistical analysis was performed using GraphPad Prism (GraphPad). Statistical tests used were: unpaired t-test for two group-comparisons or chi-square test or One-Way analysis of variances (ANOVA) followed by an appropriate multiple comparison procedure for comparisons comprising more than two groups. Correlation analysis was performed according to Pearson test. Data are expressed as mean ± SEM, $n \geq 5$ for all groups. Differences between groups were considered significant if P-values were < 0.05.

Table 1: Primary antibodies used for IHC

Antibody	Species	Company	Dilution
Anti-Chromogranin A	Rabbit (ab15160)	Abcam	1:100
Anti-Dclk1	Rabbit	Biomol	1:100
Anti-GLP-1	Rabbit (2760S)	CST	1:200
Anti-Serotonin (5-HT)	Rat (ab6336)	Abcam	1:150

Table 2: Secondary antibodies used for IHC

Antibody	Company	Dilution
HRP conjugated donkey anti rabbit IgG	Dianova (711-035-152)	1:300
HRP conjugated goat anti rat IgG	Dianova (112-035-003)	1:300

Table 3: Primer sequences and probes

	Mouse		
Target genes	**Forward primer**	**Reverse primer**	**Probe**
Ahr	gcaagaaggagagttcttgttacag	aaagcccaggtaatcttggata	69
Aldob	cgtgctgtgttgaggattgc	atagcgagccagagcattgg	11
Alpi	catctccaacatggacattga	ggttccagactggttactgtca	109
Atoh1	gggttgtagtggacgagctt	gcttctgtaccccattcacc	11
Atp5e	cggttttcccagatctgtgc	cccgaagtcttctcagcgtt	112
Arx	caggagagaggagcagaggt	actgattgctcatggctggt	117
Cck	tgatttccccatccaaagc	gcttctgcagggactaccg	9
Cd24a	ctggggttgctgcttctg	caacagatgtttggttgcagtaa	68
ChgA	ggaggctgtggctacacaca	ccatccactgcctgagagtc	89
Chpt1	aggaggcaccatactggaca	tcccatcaatggcatccagt	95
Cox7a1	gctcatctaccagaagccact	gtcattgtcggcctggaaga	53
Ddit4	ccagagaagagggccttga	ccatccaggtatgaggagtctt	80
Dclk1	ttcaacacaggccccaag	ccttatcaagagcggtggtt	18
Dpp4	tgggaacactggaagttgaa	cgcttgctatccacaaatcc	71
Eno3	acaaagcacgatacctgggg	ttccagcagagcaggaccta	161
Fasn	cccaccctgatttctgccat	cacctaggccaccagtgatg	23
Fbp2	tgcaggtgtgtcttcaacga	gcctccctttgctccttgta	74
Foxa1	acagggttggatggttgtgt	tgctctcatgcccttccatc	36
Gcg	ccagtgatgtgagttcttacttgg	caatggcgacttcttctgg	27
Gfi1	atcaagcctgccacgagaag	ctcctctgatggcaccacag	9
Gip	tctcagggaaaggaggacaa	tcagcacatcatcatcactgag	98
Glud1	atcaagccctgcaaccatgt	tagccttcgatgacctccca	60
Gpx2	gttctcggcttcccttgc	ttcaggatctcctcgttctga	2
Gsr	ccaaggtggcctcaaacaac	gcaggcctagaattccagca	78
G6pdx	gagccacccatctttccaca	aggggcagactgataggcat	11

Table 3 continued

Mouse			
Target genes	**Forward primer**	**Reverse primer**	**Probe**
Hadh	tggatactacaaagttcatcttgga	aaggactgggctgaaataagg	106
Hes1	acaccggacaaaccaaagac	cgcctcttctccatgatagg	99
Hk2	ttcaccttctccttcccttg	ccctttgtccacttgaggag	64
Hmgcr	tgattggagttggcaccat	tggccaacactgacatgc	78
Hmgcs2	gtaacggggagcactgagag	ccaaccgtttccatacccca	110
Hprt	tcctcctcagaccgctttt	cctggttcatcatcgctaatc	95
Isl1	tgccctgtagctggtttctc	gaaataaagaaaaggaaagaaaaggat	91
Klf4	ctgaaggcgtctctgaccac	cgtctgggcttcctttgcta	66
Krt20	ggttcaagtcacggagctga	ttcatgctgaggtgggactg	80
Ldhb	ggcagagaagcttggcatt	agactcctgccacattcacc	3
Lgr5	cttcactcggtgcagtgct	cagccagctaccaaataggtg	60
Lmx1a	ctcaccccgaacatgttgga	ccgaggtctcaatcgcactt	25
Lpl	ctcgctctcagatgccctac	ggttgtgttgcttgccatt	95
Lyz1	ggcaaaaccccaagatctaa	tctctcaccaccctctttgc	46
Mcp2	cactgtgttgatggctacagg	caaatccgaaacagctgagag	18
Mtor	tctggtaactgaggcctgga	gtccactggaagcacagaca	52
Muc2	ggcagtacaagaaccggagt	ggtctggcagtcctcgaa	66
Neurog3	aaactccaaagggtggatga	tgtgccagcctctgacttag	93
Parl	tgcatcgggagcaatcatga	atgatagcgagcctcccctc	112
Pax4	ctctgtgaagctctggaccc	gtttgctggtggtctggtct	78
Pax6	ttgcataagaggcatcggct	cagcaccgaaagcaagacac	78
Pck1	aaatgctttgcgttgcggat	tgcccaggatcagcatatgc	69
Pcsk1	tggagttgcatataattccaaagtt	agcctcaatggcatcagttac	42
Pdha1	catcgttggagctcaggtg	cgccgtataatgtcaaacagac	15
Pdk4	cgcttagtgaacactccttcg	cttctgggctcttctcatgg	22
Pkm2	gcaggaaccgaagtacgc	tgtgttccaggaaggtgtca	3
Prom1	cagcggcagaagcagaat	tggttagccacaaagccata	69
Pyy	cctaccctgccaaaccag	ggacatctctttttccataccg	17
Sgk1	acacgctgaagttcagtcca	aggagaggggttagcgttca	92
Slc37a2	tgctgcatcatgctgatctt	cccattctggccaatgtagt	32
Slc7a11	tgggtggaactgctcgtaat	aggatgtagcgtccaaatgc	1
Sox9	gtacccgcatctgcacaac	ctcctccacgaagggtctct	66
Spdef	cctcctggtccctgaggt	cagtgaatgtggccctgac	40
Stk11	cttcatccaccgcatcgact	tcaggtacttgccgatgagc	28
Tff3	gtaacaaccgtggctgctg	gagcctggacagcttcaaaa	109
Tgfbr2	tggctctggtactctgggaa	gaaccaaatgggggctcgta	7
Tph1	ggctatcgggaagacaacat	cggatggaaaacccagtg	88
Trib3	gtcgctttgtcttcagcaact	tcatctgatccagtcatcacg	67
Yy1	ctggagaaaagccctttcag	gtcgaaggggcacacatag	94

Human			
Target genes	**Forward primer**	**Reverse primer**	**Probe**
HPRT1	tgatagatccattcctatgactgtaga	caagacattcttccagttaaagt	22
LGR5	accagactatgcctttggaaac	tcccagggagtggattctatt	78
TRIB3	gtcttcgctgaccgtgaga	cagtcagcacgcaggagtc	67

6 References

1. Zietek T, Daniel H. Intestinal Nutrient Sensing and Blood Glucose Control. *Current opinion in clinical nutrition and metabolic care* (2015) 18(4):381-8. Epub 2015/05/24. doi: 10.1097/MCO.0000000000000187.

2. Worthington JJ. The Intestinal Immunoendocrine Axis: Novel Cross-Talk between Enteroendocrine Cells and the Immune System During Infection and Inflammatory Disease. *Biochemical Society transactions* (2015) 43(4):727-33. Epub 2015/11/10. doi: 10.1042/BST20150090.

3. Clavel T, Haller D. Bacteria- and Host-Derived Mechanisms to Control Intestinal Epithelial Cell Homeostasis: Implications for Chronic Inflammation. *Inflamm Bowel Dis* (2007) 13(9):1153-64. Epub 2007/05/04. doi: 10.1002/ibd.20174.

4. Helander HF, Fandriks L. Surface Area of the Digestive Tract - Revisited. *Scandinavian journal of gastroenterology* (2014) 49(6):681-9. Epub 2014/04/04. doi: 10.3109/00365521.2014.898326.

5. Barker N. Adult Intestinal Stem Cells: Critical Drivers of Epithelial Homeostasis and Regeneration. *Nat Rev Mol Cell Biol* (2014) 15(1):19-33. doi: 10.1038/nrm3721.

6. Barker N, Clevers H. Leucine-Rich Repeat-Containing G-Protein-Coupled Receptors as Markers of Adult Stem Cells. *Gastroenterology* (2010) 138(5):1681-96. doi: 10.1053/j.gastro.2010.03.002.

7. Sartor RB. Mechanisms of Disease: Pathogenesis of Crohn's Disease and Ulcerative Colitis. *Nat Clin Pract Gastroenterol Hepatol* (2006) 3(7):390-407.

8. Cadwell K, Liu JY, Brown SL, Miyoshi H, Loh J, Lennerz JK, et al. A Key Role for Autophagy and the Autophagy Gene Atg16l1 in Mouse and Human Intestinal Paneth Cells. *Nature* (2008) 456(7219):259-63. doi: 10.1038/nature07416.

9. Khaloian S, Rath E, Hammoudi N, Gleisinger E, Blutke A, Giesbertz P, et al. Mitochondrial Impairment Drives Intestinal Stem Cell Transition into Dysfunctional Paneth Cells Predicting Crohn's Disease Recurrence. *Gut* (2020) 69(11):1939-51. Epub 20200228. doi: 10.1136/gutjnl-2019-319514.

10. Wang H, Steeds J, Motomura Y, Deng Y, Verma-Gandhu M, El-Sharkawy RT, et al. Cd4+ T Cell-Mediated Immunological Control of Enterochromaffin Cell Hyperplasia and 5-Hydroxytryptamine Production in Enteric Infection. *Gut* (2007) 56(7):949-57. doi: 10.1136/gut.2006.103226.

11. Worthington JJ, Samuelson LC, Grencis RK, McLaughlin JT. Adaptive Immunity Alters Distinct Host Feeding Pathways During Nematode Induced Inflammation, a Novel Mechanism in Parasite Expulsion. *PLoS Pathog* (2013) 9(1):e1003122. doi: 10.1371/journal.ppat.1003122.

12. Gerbe F, Sidot E, Smyth DJ, Ohmoto M, Matsumoto I, Dardalhon V, et al. Intestinal Epithelial Tuft Cells Initiate Type 2 Mucosal Immunity to Helminth Parasites. *Nature* (2016) 529(7585):226-30. doi: 10.1038/nature16527.

13. van der Post S, Jabbar KS, Birchenough G, Arike L, Akhtar N, Sjovall H, et al. Structural Weakening of the Colonic Mucus Barrier Is an Early Event in Ulcerative Colitis Pathogenesis. *Gut* (2019) 68(12):2142-51. Epub 20190326. doi: 10.1136/gutjnl-2018-317571.

14. Rath E, Haller D. Intestinal Epithelial Cell Metabolism at the Interface of Microbial Dysbiosis and Tissue Injury. *Mucosal Immunol* (2022) 15(4):595-604. Epub 20220509. doi: 10.1038/s41385-022-00514-x.

15. Rath E, Moschetta A, Haller D. Mitochondrial Function - Gatekeeper of Intestinal Epithelial Cell Homeostasis. *Nat Rev Gastroenterol Hepatol* (2018) 15(8):497-516. doi: 10.1038/s41575-018-0021-x.

16. Urbauer E, Rath E, Haller D. Mitochondrial Metabolism in the Intestinal Stem Cell Niche-Sensing and Signaling in Health and Disease. *Front Cell Dev Biol* (2020) 8:602814. Epub 20210105. doi: 10.3389/fcell.2020.602814.

17. Ludikhuize MC, Meerlo M, Gallego MP, Julià MB, Nguyen NTB, Brombacher EC, et al. Mitochondria Define Intestinal Stem Cell Differentiation Downstream of a Foxo/Notch Axis. *bioRxiv* (2019):777391. doi: 10.1101/777391.

18. Haberman Y, Karns R, Dexheimer PJ, Schirmer M, Somekh J, Jurickova I, et al. Ulcerative Colitis Mucosal Transcriptomes Reveal Mitochondriopathy and Personalized Mechanisms Underlying Disease Severity and Treatment Response. *Nat Commun* (2019) 10(1):38. doi: 10.1038/s41467-018-07841-3.

19. Mottawea W, Chiang CK, Muhlbauer M, Starr AE, Butcher J, Abujamel T, et al. Altered Intestinal Microbiota-Host Mitochondria Crosstalk in New Onset Crohn's Disease. *Nat Commun* (2016) 7:13419. doi: 10.1038/ncomms13419.

20. Denson LA. Mitochondrial Networks: A New Therapeutic Target in Colitis. *Cell Mol Gastroenterol Hepatol* (2020) 10(2):426-7. doi: 10.1016/j.jcmgh.2020.05.008.

21. Mancini NL, Goudie L, Xu W, Sabouny R, Rajeev S, Wang A, et al. Perturbed Mitochondrial Dynamics Is a Novel Feature of Colitis That Can Be Targeted to Lessen Disease. *Cell Mol Gastroenterol Hepatol* (2020) 10(2):287-307. doi: 10.1016/j.jcmgh.2020.04.004.

22. Rath E, Haller D. Mitochondria at the Interface between Danger Signaling and Metabolism: Role of Unfolded Protein Responses in Chronic Inflammation. *Inflamm Bowel Dis* (2012) 18(7):1364-77. doi: 10.1002/ibd.21944.

23. Jackson DN, Theiss AL. Gut Bacteria Signaling to Mitochondria in Intestinal Inflammation and Cancer. *Gut Microbes* (2020) 11(3):285-304. doi: 10.1080/19490976.2019.1592421.

24. Friedrich M, Diegelmann J, Schauber J, Auernhammer CJ, Brand S. Intestinal Neuroendocrine Cells and Goblet Cells Are Mediators of Il-17a-Amplified Epithelial Il-17c Production in Human Inflammatory Bowel Disease. *Mucosal Immunol* (2015) 8(4):943-58. doi: 10.1038/mi.2014.124.

25. Sakiyama T, Fujita H, Tsubouchi H. Autoantibodies against Ubiquitination Factor E4a (Ube4a) Are Associated with Severity of Crohn's Disease. *Inflammatory bowel diseases* (2008) 14(3):310-7. doi: 10.1002/ibd.20328.

26. Zietek T, Rath E. Inflammation Meets Metabolic Disease: Gut Feeling Mediated by Glp-1. *Front Immunol* (2016) 7:154. Epub 20160422. doi: 10.3389/fimmu.2016.00154.

27. Massironi S, Zilli A, Cavalcoli F, Conte D, Peracchi M. Chromogranin a and Other Enteroendocrine Markers in Inflammatory Bowel Disease. *Neuropeptides* (2016) 58:127-34. Epub 20160112. doi: 10.1016/j.npep.2016.01.002.

28. Hadjiyanni I, Siminovitch KA, Danska JS, Drucker DJ. Glucagon-Like Peptide-1 Receptor Signalling Selectively Regulates Murine Lymphocyte Proliferation and Maintenance of Peripheral Regulatory T Cells. *Diabetologia* (2010) 53(4):730-40.

29. Yusta B, Baggio LL, Koehler J, Holland D, Cao X, Pinnell LJ, et al. Glp-1r Agonists Modulate Enteric Immune Responses through the Intestinal Intraepithelial Lymphocyte Glp-1r. *Diabetes* (2015) 64(7):2537-49. Epub 2015/03/05. doi: 10.2337/db14-1577.

30. Moran GW, Leslie FC, McLaughlin JT. Crohn's Disease Affecting the Small Bowel Is Associated with Reduced Appetite and Elevated Levels of Circulating Gut Peptides. *Clin Nutr* (2013) 32(3):404-11. Epub 2012/09/25. doi: 10.1016/j.clnu.2012.08.024.

31. Keller J, Binnewies U, Rosch M, Juul Holst J, Beglinger C, Andresen V, et al. Gastric Emptying and Disease Activity in Inflammatory Bowel Disease. *European journal of clinical investigation* (2015). Epub 2015/10/02. doi: 10.1111/eci.12542.

32. El-Salhy M, Hatlebakk JG. Changes in Enteroendocrine and Immune Cells Following Colitis Induction by Tnbs in Rats. *Mol Med Rep* (2016) 14(6):4967-74. Epub 20161031. doi: 10.3892/mmr.2016.5902.

33. El-Salhy M, Umezawa K, Hatlebakk JG, Gilja OH. Abnormal Differentiation of Stem Cells into Enteroendocrine Cells in Rats with Dss-Induced Colitis. *Mol Med Rep* (2017) 15(4):2106-12. Epub 20170301. doi: 10.3892/mmr.2017.6266.

34. Zatorski H, Salaga M, Zielinska M, Mokrowiecka A, Jacenik D, Krajewska WM, et al. Colonic Inflammation Induces Changes in Glucose Levels through Modulation of Incretin System. *Pharmacol Rep* (2021) 73(6):1670-9. Epub 20210917. doi: 10.1007/s43440-021-00327-y.

35. Kong L, Pokatayev V, Lefkovith A, Carter GT, Creasey EA, Krishna C, et al. The Landscape of Immune Dysregulation in Crohn's Disease Revealed through Single-Cell Transcriptomic Profiling in the Ileum and Colon. *Immunity* (2023) 56(2):444-58 e5. Epub 20230130. doi: 10.1016/j.immuni.2023.01.002.

36. Metwaly A, Jovic J, Waldschmitt N, Khaloian S, Heimes H, Hacker D, et al. Diet Prevents the Expansion of Segmented Filamentous Bacteria and Ileo-Colonic Inflammation in a Model of Crohn's Disease. *Microbiome* (2023) 11(1):66. Epub 20230331. doi: 10.1186/s40168-023-01508-y.

37. Yoon H, Schaubeck M, Lagkouvardos I, Blesl A, Heinzlmeir S, Hahne H, et al. Increased Pancreatic Protease Activity in Response to Antibiotics Impairs Gut Barrier and Triggers Colitis. *Cell Mol Gastroenterol Hepatol* (2018) 6(3):370-88 e3. Epub 20180529. doi: 10.1016/j.jcmgh.2018.05.008.

38. Waldschmitt N, Berger E, Rath E, Sartor RB, Weigmann B, Heikenwalder M, et al. C/Ebp Homologous Protein Inhibits Tissue Repair in Response to Gut Injury and Is Inversely Regulated with Chronic Inflammation. *Mucosal Immunol* (2014) 7(6):1452-66. Epub 20140521. doi: 10.1038/mi.2014.34.

39. Schaubeck M, Clavel T, Calasan J, Lagkouvardos I, Haange SB, Jehmlich N, et al. Dysbiotic Gut Microbiota Causes Transmissible Crohn's Disease-Like Ileitis Independent of Failure in Antimicrobial Defence. *Gut* (2016) 65(2):225-37. doi: 10.1136/gutjnl-2015-309333.

40. Keubler LM, Buettner M, Hager C, Bleich A. A Multihit Model: Colitis Lessons from the Interleukin-10-Deficient Mouse. *Inflamm Bowel Dis* (2015) 21(8):1967-75. doi: 10.1097/MIB.0000000000000468.

41. Eri R, McGuckin MA, Wadley R. T Cell Transfer Model of Colitis: A Great Tool to Assess the Contribution of T Cells in Chronic Intestinal Inflammation. *Methods Mol Biol* (2012) 844:261-75. doi: 10.1007/978-1-61779-527-5_19.

42. Crepin VF, Collins JW, Habibzay M, Frankel G. Citrobacter Rodentium Mouse Model of Bacterial Infection. *Nat Protoc* (2016) 11(10):1851-76. Epub 20160908. doi: 10.1038/nprot.2016.100.

43. Jenkins BR, Blaseg NA, Grifka-Walk HM, Deuling B, Swain SD, Campbell EL, et al. Loss of Interleukin-10 Receptor Disrupts Intestinal Epithelial Cell Proliferation and Skews Differentiation Towards the Goblet Cell Fate. *FASEB J* (2021) 35(6):e21551. doi: 10.1096/fj.202002369R.

44. Kanke M, Kennedy Ng MM, Connelly S, Singh M, Schaner M, Shanahan MT, et al. Single-Cell Analysis Reveals Unexpected Cellular Changes and Transposon Expression Signatures in the Colonic Epithelium of Treatment-Naive Adult Crohn's Disease Patients. *Cell Mol Gastroenterol Hepatol* (2022) 13(6):1717-40. Epub 20220212. doi: 10.1016/j.jcmgh.2022.02.005.

45. Erben U, Loddenkemper C, Doerfel K, Spieckermann S, Haller D, Heimesaat MM, et al. A Guide to Histomorphological Evaluation of Intestinal Inflammation in Mouse Models. *Int J Clin Exp Pathol* (2014) 7(8):4557-76. Epub 20140715.

46. Okumura M, Hamada A, Ohsaka F, Tsuruta T, Hira T, Sonoyama K. Expression of Serotonin Receptor Htr4 in Glucagon-Like Peptide-1-Positive Enteroendocrine Cells of the Murine Intestine. *Pflugers Arch* (2020) 472(10):1521-32. Epub 20200901. doi: 10.1007/s00424-020-02453-7.

47. Lund ML, Egerod KL, Engelstoft MS, Dmytriyeva O, Theodorsson E, Patel BA, et al. Enterochromaffin 5-Ht Cells - a Major Target for Glp-1 and Gut Microbial Metabolites. *Mol Metab* (2018) 11:70-83. Epub 20180310. doi: 10.1016/j.molmet.2018.03.004.

48. Lund ML, Sorrentino G, Egerod KL, Kroone C, Mortensen B, Knop FK, et al. L-Cell Differentiation Is Induced by Bile Acids through Gpbar1 and Paracrine Glp-1 and Serotonin Signaling. *Diabetes* (2020) 69(4):614-23. Epub 20200210. doi: 10.2337/db19-0764.

49. Jenny M, Uhl C, Roche C, Duluc I, Guillermin V, Guillemot F, et al. Neurogenin3 Is Differentially Required for Endocrine Cell Fate Specification in the Intestinal and Gastric Epithelium. *EMBO J* (2002) 21(23):6338-47. doi: 10.1093/emboj/cdf649.

50. Ingersoll SA, Ayyadurai S, Charania MA, Laroui H, Yan Y, Merlin D. The Role and Pathophysiological Relevance of Membrane Transporter Pept1 in Intestinal Inflammation and Inflammatory Bowel Disease. *Am J Physiol Gastrointest Liver Physiol* (2012) 302(5):G484-92. doi: 10.1152/ajpgi.00477.2011.

51. Ogura Y, Bonen DK, Inohara N, Nicolae DL, Chen FF, Ramos R, et al. A Frameshift Mutation in Nod2 Associated with Susceptibility to Crohn's Disease. *Nature* (2001) 411(6837):603-6. doi: 10.1038/35079114.

52. Zucchelli M, Torkvist L, Bresso F, Halfvarson J, Hellquist A, Anedda F, et al. Pept1 Oligopeptide Transporter (Slc15a1) Gene Polymorphism in Inflammatory Bowel Disease. *Inflamm Bowel Dis* (2009) 15(10):1562-9. doi: 10.1002/ibd.20963.

53. Lebrun LJ, Lenaerts K, Kiers D, Pais de Barros JP, Le Guern N, Plesnik J, et al. Enteroendocrine L Cells Sense Lps after Gut Barrier Injury to Enhance Glp-1 Secretion. *Cell Rep* (2017) 21(5):1160-8. doi: 10.1016/j.celrep.2017.10.008.

54. Petersen N, Reimann F, Bartfeld S, Farin HF, Ringnalda FC, Vries RG, et al. Generation of L Cells in Mouse and Human Small Intestine Organoids. *Diabetes* (2014) 63(2):410-20. Epub 20131015. doi: 10.2337/db13-0991.

55. Smirnova MG, Guo L, Birchall JP, Pearson JP. Lps up-Regulates Mucin and Cytokine Mrna Expression and Stimulates Mucin and Cytokine Secretion in Goblet Cells. *Cell Immunol* (2003) 221(1):42-9. doi: 10.1016/s0008-8749(03)00059-5.

56. Delmotte P, Marin Mathieu N, Sieck GC. Tnfalpha Induces Mitochondrial Fragmentation and Biogenesis in Human Airway Smooth Muscle. *Am J Physiol Lung Cell Mol Physiol* (2021) 320(1):L137-L51. Epub 20201104. doi: 10.1152/ajplung.00305.2020.

57. Shinde A, Jung H, Lee H, Singh K, Roy M, Gohel D, et al. Tnf-Alpha Differentially Modulates Subunit Levels of Respiratory Electron Transport Complexes of Er/Pr +Ve/-Ve Breast Cancer Cells to Regulate Mitochondrial Complex Activity and Tumorigenic Potential. *Cancer Metab* (2021) 9(1):19. Epub 20210429. doi: 10.1186/s40170-021-00254-9.

58. Berger E, Rath E, Yuan D, Waldschmitt N, Khaloian S, Allgauer M, et al. Mitochondrial Function Controls Intestinal Epithelial Stemness and Proliferation. *Nat Commun* (2016) 7:13171. doi: 10.1038/ncomms13171.

59. Urbauer E, Aguanno D, Mindermann N, Omer H, Metwaly A, Krammel T, et al. Mitochondrial Perturbation in the Intestine Causes Microbiota-Dependent Injury and Gene Signatures Discriminative of Inflammatory Disease. *Cell Host Microbe* (2024) 32(8):1347-64 e10. Epub 20240715. doi: 10.1016/j.chom.2024.06.013.

60. Martin FP, Rezzi S, Philippe D, Tornier L, Messlik A, Holzlwimmer G, et al. Metabolic Assessment of Gradual Development of Moderate Experimental Colitis in Il-10 Deficient Mice. *J Proteome Res* (2009) 8(5):2376-87. doi: 10.1021/pr801006e.

61. Deleyto-Seldas N, Efeyan A. The Mtor-Autophagy Axis and the Control of Metabolism. *Front Cell Dev Biol* (2021) 9:655731. Epub 20210701. doi: 10.3389/fcell.2021.655731.

62. Ip WKE, Hoshi N, Shouval DS, Snapper S, Medzhitov R. Anti-Inflammatory Effect of Il-10 Mediated by Metabolic Reprogramming of Macrophages. *Science* (2017) 356(6337):513-9. doi: 10.1126/science.aal3535.

63. Urbauer E. Mitochondrial Function in the Regulation of Epithelial Cell Homeostasis – Impact on Intestinal Pathologies: Technische Universität München (2024).

64. Becker C, Kukat A, Szczepanowska K, Hermans S, Senft K, Brandscheid CP, et al. Clpp Deficiency Protects against Metabolic Syndrome but Hinders Adaptive Thermogenesis. *EMBO Rep* (2018) 19(5). Epub 20180327. doi: 10.15252/embr.201745126.

65. Bhaskaran S, Pharaoh G, Ranjit R, Murphy A, Matsuzaki S, Nair BC, et al. Loss of Mitochondrial Protease Clpp Protects Mice from Diet-Induced Obesity and Insulin Resistance. *EMBO Rep* (2018) 19(3). Epub 20180202. doi: 10.15252/embr.201745009.

66. Panaro BL, Yusta B, Matthews D, Koehler JA, Song Y, Sandoval DA, et al. Intestine-Selective Reduction of Gcg Expression Reveals the Importance of the Distal Gut for Glp-1 Secretion. *Mol Metab* (2020) 37:100990. Epub 20200409. doi: 10.1016/j.molmet.2020.100990.

67. Wichmann A, Allahyar A, Greiner TU, Plovier H, Lunden GO, Larsson T, et al. Microbial Modulation of Energy Availability in the Colon Regulates Intestinal Transit. *Cell Host Microbe* (2013) 14(5):582-90. doi: 10.1016/j.chom.2013.09.012.

68. Nguyen AT, Mandard S, Dray C, Deckert V, Valet P, Besnard P, et al. Lipopolysaccharides-Mediated Increase in Glucose-Stimulated Insulin Secretion: Involvement of the Glp-1 Pathway. *Diabetes* (2014) 63(2):471-82. doi: 10.2337/db13-0903.

69. Williams L, Alshehri A, Robichaud B, Cudmore A, Gagnon J. The Role of the Bacterial Muramyl Dipeptide in the Regulation of Glp-1 and Glycemia. *Int J Mol Sci* (2020) 21(15). Epub 20200724. doi: 10.3390/ijms21155252.

70. Gribble FM, Reimann F. Enteroendocrine Cells: Chemosensors in the Intestinal Epithelium. *Annual review of physiology* (2016) 78:277-99. Epub 2015/10/08. doi: 10.1146/annurev-physiol-021115-105439.

71. Gagnon J, Sauve M, Zhao W, Stacey HM, Wiber SC, Bolz SS, et al. Chronic Exposure to Tnfalpha Impairs Secretion of Glucagon-Like Peptide-1. *Endocrinology* (2015) 156(11):3950-60. Epub 2015/08/14. doi: 10.1210/en.2015-1361.

72. Selleri S, Palazzo M, Deola S, Wang E, Balsari A, Marincola FM, et al. Induction of Pro-Inflammatory Programs in Enteroendocrine Cells by the Toll-Like Receptor Agonists Flagellin and Bacterial Lps. *International immunology* (2008) 20(8):961-70. Epub 2008/06/12. doi: 10.1093/intimm/dxn055.

73. Bogunovic M, Dave SH, Tilstra JS, Chang DT, Harpaz N, Xiong H, et al. Enteroendocrine Cells Express Functional Toll-Like Receptors. *Am J Physiol Gastrointest Liver Physiol* (2007) 292(6):G1770-83. doi: 10.1152/ajpgi.00249.2006.

74. Moran GW, Leslie FC, Levison SE, Worthington J, McLaughlin JT. Enteroendocrine Cells: Neglected Players in Gastrointestinal Disorders? *Therapeutic advances in gastroenterology* (2008) 1(1):51-60. Epub 2008/07/01. doi: 10.1177/1756283X08093943.

75. Worthington JJ, Reimann F, Gribble FM. Enteroendocrine Cells-Sensory Sentinels of the Intestinal Environment and Orchestrators of Mucosal Immunity. *Mucosal Immunol* (2018) 11(1):3-20. Epub 20170830. doi: 10.1038/mi.2017.73.

76. Habib AM, Richards P, Cairns LS, Rogers GJ, Bannon CA, Parker HE, et al. Overlap of Endocrine Hormone Expression in the Mouse Intestine Revealed by Transcriptional Profiling and Flow Cytometry. *Endocrinology* (2012) 153(7):3054-65. Epub 2012/06/12. doi: 10.1210/en.2011-2170.

77. Egerod KL, Engelstoft MS, Grunddal KV, Nohr MK, Secher A, Sakata I, et al. A Major Lineage of Enteroendocrine Cells Coexpress Cck, Secretin, Gip, Glp-1, Pyy, and Neurotensin but Not Somatostatin. *Endocrinology* (2012) 153(12):5782-95. Epub 2012/10/16. doi: 10.1210/en.2012-1595.

78. Sykaras AG, Demenis C, Cheng L, Pisitkun T, McLaughlin JT, Fenton RA, et al. Duodenal Cck Cells from Male Mice Express Multiple Hormones Including Ghrelin. *Endocrinology* (2014) 155(9):3339-51. Epub 2014/07/09. doi: 10.1210/en.2013-2165.

79. Fothergill LJ, Furness JB. Diversity of Enteroendocrine Cells Investigated at Cellular and Subcellular Levels: The Need for a New Classification Scheme. *Histochem Cell Biol* (2018) 150(6):693-702. Epub 20181024. doi: 10.1007/s00418-018-1746-x.

80. Gehart H, van Es JH, Hamer K, Beumer J, Kretzschmar K, Dekkers JF, et al. Identification of Enteroendocrine Regulators by Real-Time Single-Cell Differentiation Mapping. *Cell* (2019) 176(5):1158-73 e16. Epub 20190131. doi: 10.1016/j.cell.2018.12.029.

81. Drucker DJ, Habener JF, Holst JJ. Discovery, Characterization, and Clinical Development of the Glucagon-Like Peptides. *J Clin Invest* (2017) 127(12):4217-27. Epub 20171201. doi: 10.1172/JCI97233.

82. Lee SJ, Lee J, Li KK, Holland D, Maughan H, Guttman DS, et al. Disruption of the Murine Glp2r Impairs Paneth Cell Function and Increases Susceptibility to Small Bowel Enteritis. *Endocrinology* (2012) 153(3):1141-51. doi: 10.1210/en.2011-1954.

83. Qi KK, Wu J, Wan J, Men XM, Xu ZW. Purified Pegylated Porcine Glucagon-Like Peptide-2 Reduces the Severity of Colonic Injury in a Murine Model of Experimental Colitis. *Peptides* (2014) 52:11-8. doi: 10.1016/j.peptides.2013.11.012.

84. Boushey RP, Yusta B, Drucker DJ. Glucagon-Like Peptide 2 Decreases Mortality and Reduces the Severity of Indomethacin-Induced Murine Enteritis. *Am J Physiol* (1999) 277(5 Pt 1):E937-47.

85. Alavi K, Schwartz MZ, Palazzo JP, Prasad R. Treatment of Inflammatory Bowel Disease in a Rodent Model with the Intestinal Growth Factor Glucagon-Like Peptide-2. *J Pediatr Surg* (2000) 35(6):847-51. doi: 10.1053/jpsu.2000.6861.

86. Drucker DJ, Yusta B, Boushey RP, DeForest L, Brubaker PL. Human [Gly2]Glp-2 Reduces the Severity of Colonic Injury in a Murine Model of Experimental Colitis. *Am J Physiol* (1999) 276(1 Pt 1):G79-91.

87. Buchman AL, Katz S, Fang JC, Bernstein CN, Abou-Assi SG, Teduglutide Study G. Teduglutide, a Novel Mucosally Active Analog of Glucagon-Like Peptide-2 (Glp-2) for the Treatment of Moderate to Severe Crohn's Disease. *Inflamm Bowel Dis* (2010) 16(6):962-73. doi: 10.1002/ibd.21117.

88. Urbauer E, Aguanno D, Mindermann N, Omer H, Metwaly A, Krammel T, et al. Mitochondrial Perturbation in the Intestine Causes Microbiota-Dependent Injury and Gene Signatures Discriminative of Inflammatory Disease. *bioRxiv* (2024):2023.07.27.549844. doi: 10.1101/2023.07.27.549844.

89. Huang C, Wang J, Liu H, Huang R, Yan X, Song M, et al. Ketone Body Beta-Hydroxybutyrate Ameliorates Colitis by Promoting M2 Macrophage Polarization through the Stat6-Dependent Signaling Pathway. *BMC Med* (2022) 20(1):148. Epub 20220415. doi: 10.1186/s12916-022-02352-x.

90. Weber-Stiehl S, Taubenheim J, Jarke L, Rocken C, Schreiber S, Aden K, et al. Hexokinase 2 Expression in Apical Enterocytes Correlates with Inflammation Severity in Patients with Inflammatory Bowel Disease. *BMC Med* (2024) 22(1):490. Epub 20241023. doi: 10.1186/s12916-024-03710-7.

91. Tu1826 Impact of Glp-1 Receptor Agonist on Clinical Outcomes in Patients with Crohn's Disease and Ulcerative Colitis: Insights from a Large-Scale Cohort Study. *Gastroenterology* (2024) 166(5, Supplement):S-1424-S-5. doi: https://doi.org/10.1016/S0016-5085(24)03727-2.

92. Rath E, Berger E, Messlik A, Nunes T, Liu B, Kim SC, et al. Induction of Dsrna-Activated Protein Kinase Links Mitochondrial Unfolded Protein Response to the Pathogenesis of Intestinal Inflammation. *Gut* (2011). Epub 2011/10/15. doi: 10.1136/gutjnl-2011-300767.

93. Seiferling D, Szczepanowska K, Becker C, Senft K, Hermans S, Maiti P, et al. Loss of Clpp Alleviates Mitochondrial Cardiomyopathy without Affecting the Mammalian Uprmt. *EMBO Rep* (2016) 17(7):953-64. Epub 20160506. doi: 10.15252/embr.201642077.

94. Lamas B, Michel ML, Waldschmitt N, Pham HP, Zacharioudaki V, Dupraz L, et al. Card9 Mediates Susceptibility to Intestinal Pathogens through Microbiota Modulation and Control of Bacterial Virulence. *Gut* (2018) 67(10):1836-44. Epub 20170808. doi: 10.1136/gutjnl-2017-314195.

95. Zietek T, Rath E. Chapter 3 - Intestinal Organoids: Mini-Guts Grown in the Laboratory. In: Davies JA, Lawrence ML, editors. *Organs and Organoids*. Academic Press (2018). p. 43-71.

96. Zietek T, Giesbertz P, Ewers M, Reichart F, Weinmuller M, Urbauer E, et al. Organoids to Study Intestinal Nutrient Transport, Drug Uptake and Metabolism - Update to the Human Model and Expansion of Applications. *Front Bioeng Biotechnol* (2020) 8:577656. Epub 20200911. doi: 10.3389/fbioe.2020.577656.

97. Zietek T, Rath E, Haller D, Daniel H. Intestinal Organoids for Assessing Nutrient Transport, Sensing and Incretin Secretion. *Sci Rep* (2015) 5:16831. doi: 10.1038/srep16831.